

國立交通大學

光電工程學系碩士班

碩士論文

短硫鏈分子對殼核硒化鎘/硫化鋅量子點光學性

質之研究

The Effect of Short-Chain Thiol Capping Layer on Optical  
Properties of CdSe/ZnS Quantum Dot



研究生：許安佳

指導教授：安惠榮 教授

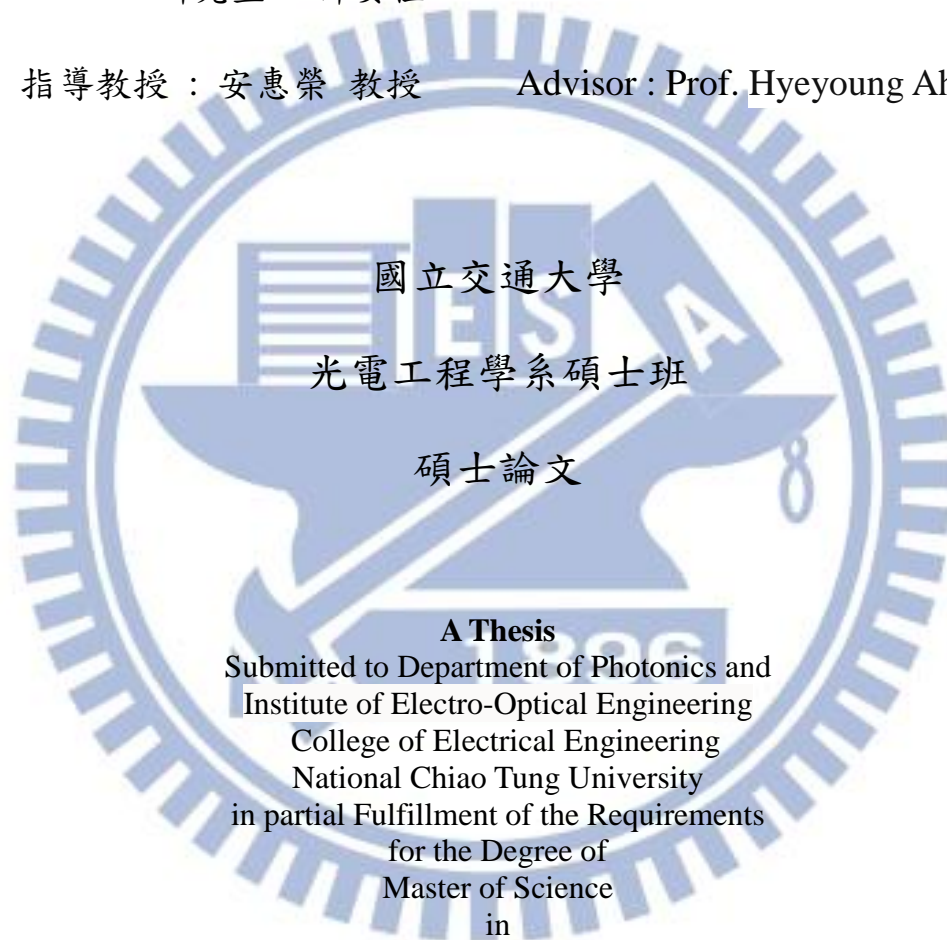
中國民國一零一年

短硫鏈分子對殼核硒化鎘/硫化鋅量子點光學性質之研究

The Effect of Short-Chain Thiol Capping Layer on Optical  
Properties of CdSe/ZnS Quantum Dot

研究生：許安佳 Student: An-Chia Hsu

指導教授：安惠榮 教授 Advisor: Prof. Hyeyoung Ahn



Institute of Electro-Optical Engineering  
June 2012

Hsinchu, Taiwan, Republic of China

中華民國一零一年六月

# The Effect of Short-Chain Thiol Capping Layer on Optical Properties of CdSe/ZnS Quantum Dot

Student: An-Chia Hsu

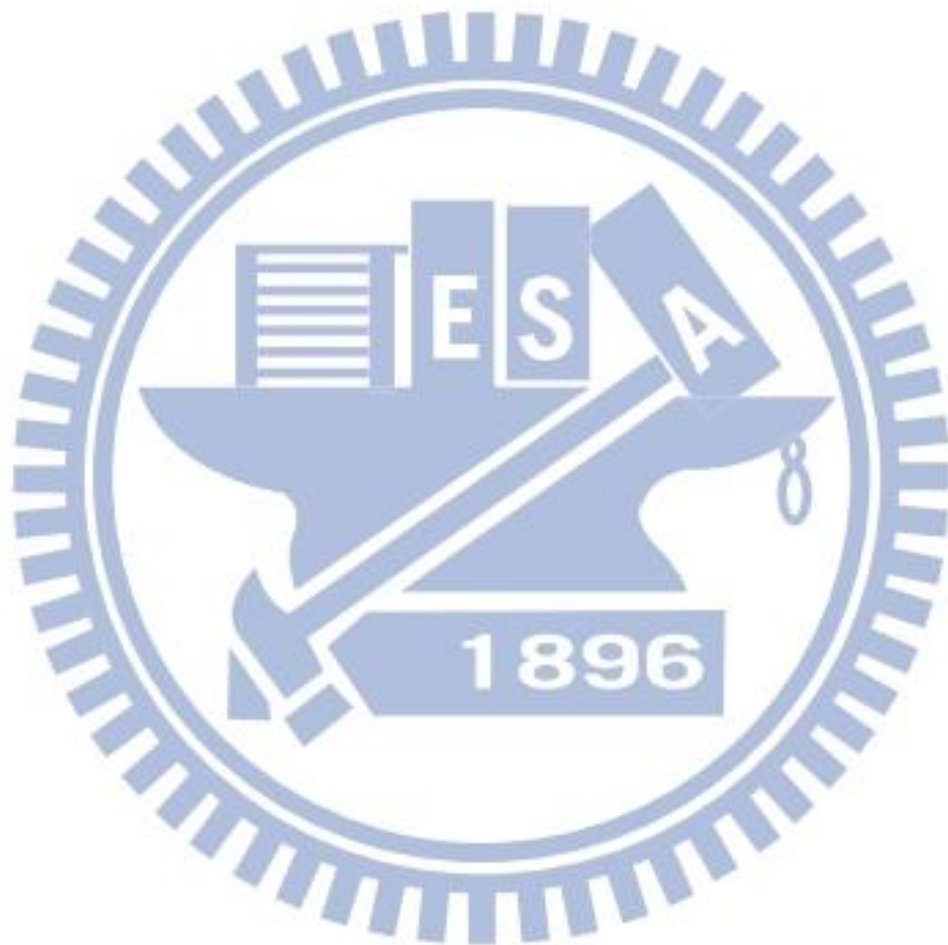
Advisor: Dr. Hyeyoung Ahn

Institute of Electro-Optical Engineering  
National Chiao Tung University

## ABSTRACT

The optical property analysis of short-chain thiol-containing molecules capping on CdSe/ZnS quantum dots (QDs) is reported. The electronic and optical properties of QDs are closely related with the highly surface-to-volume ratio and their surface electronic structure. Here we used core/shell QDs with some thiol molecules including  $\beta$ -Mercaptoethanol(BME), 3-Mercaptopropionic acid (MPA), and 1-propanethiol(NPM) to examine the effect of QD surface-thiol interaction of defect sites in short (immediately) and long (24 hr.) aging time. A comprehensive study of ultrafast spectroscopy, up conversion fluorescence, and temperature-dependent photoluminescence was used to clarify the function of thiols on QDs surface. We found the thiol molecules interact with QD only by weak coordination-type bonds through the sulfur lone-pair electrons. The thiol molecules can passivate the surface of QDs by preventing core electron from defect sites on the surface thus enhance PL intensity. While the strong covalent-type bonds are formed as thiol turn to thiolate through the long time incubation, new hole traps would be produced thus PL intensity quench. Thiol-containing molecules under investigation show different performance, which attribute to anti-oxidation, dissociation ability and second-order oxygen of the thiols.

Finally, we found that the surface passivation occurs as long as the QDs are surrounded with negative charges since thiol-/dithiol molecules have sulfur lone-pair electrons. That is the main reason why thiol-molecules usually apply to exchange ligands on the QDs surface.



# 短硫鏈分子對殼核硒化鎘/硫化鋅量子點光學性質之研究

研究生：許安佳

指導教授：安惠榮博士

光電工程學系碩士班

國立交通大學

## 摘要

本論文主要藉由由光譜及光學量測，討論含硫基的短硫鏈分子對殼核硒化鎘/硫化鋅量子點表面的影響和效用。由於量子點的表面對體積的比例極高，因此量子點的表面電子分佈結構會決定其物理性質及光學性質。此篇論文，我們使用一些硫醇分子，包括  $\beta$ -巰基乙醇 (BME)，3-巰基丙酸 (MPA) 和 1-丙硫醇 (NPM) 去測試分子和殼核量子點表面缺陷的交互作用。其中分成兩個研究的時間點：加入硫醇分子立即量測，以及加入分子後，過 24 小時再量測。我們主要只用超快吸收光譜、上轉換螢光光譜、溫度相關光致發光光譜和穩態螢光光譜來釐清硫醇分子對量子點的作用和機制。由實驗結果，可以知道硫醇分子 (thiol) 先由硫基孤對電子對 (sulfur lone-pair) 靠近量子點表面，以微弱的配位鍵形式 (coordination-type) 靠在量子點表面並減少表面缺陷，使量子點的表面鈍化 (surface passivation)，螢光強度增強 (PL enhancement)。長時間後，硫醇分子會轉為硫醇基 (thiolate)，分子改由較強的共價鍵形式 (covalent-type) 鍵結在量子點表面，但同時也產生新的缺陷，致使電洞由核內轉移出來，使螢光減弱 (PL quench)。此篇使用的硫醇分子對量子點有不同的影響，可能是抗氧化力、硫醇分子解離能力，或者是否有其餘孤對電子對作用等因素。最後，我們發現只要量子點表面附近有足夠的電子雲，就能使量子點表面鈍化。這是硫醇分子常被用來進行量子點配位體交換 (ligand exchange) 的主要原因。

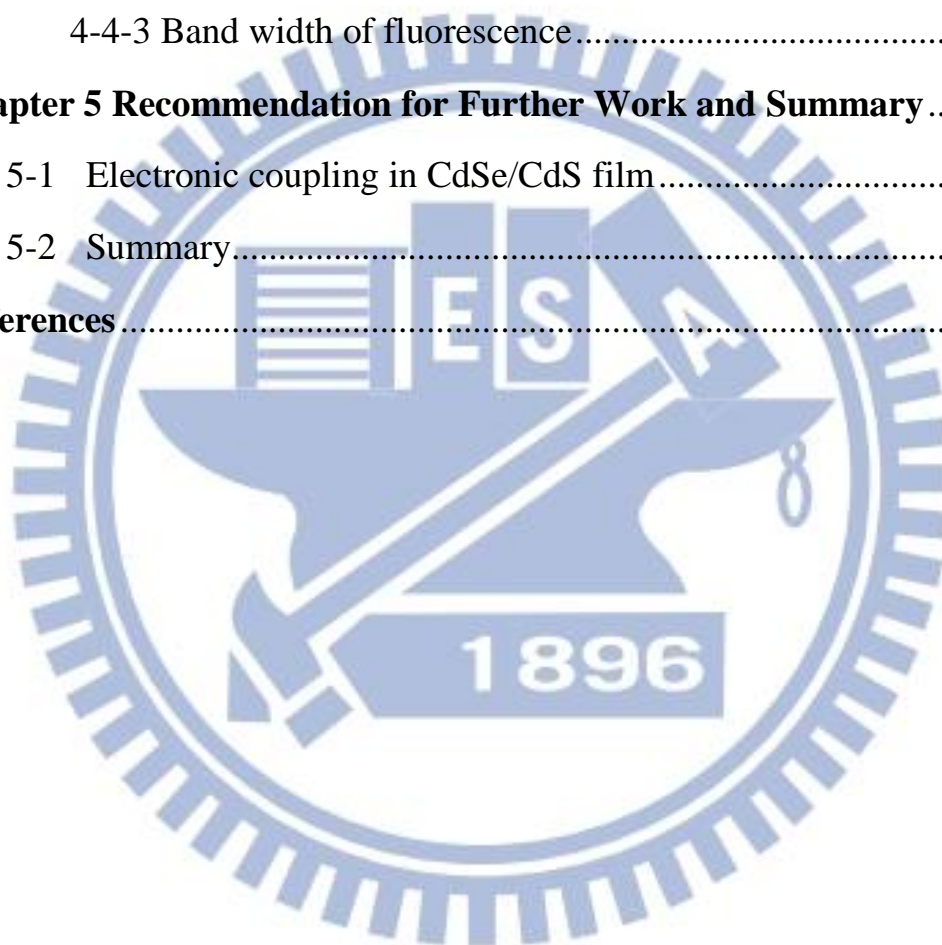
## Acknowledgement

這兩年碩士班匆匆就這樣過去了，剛進實驗室，連雷射工作原理都不懂，到現在架光路、找訊號、配樣品，樣樣輕鬆自如。這樣的成果，不斷失敗、再努力才能做到的。這兩年，湯朝暉老師提供了良好的實驗環境和資源、充分的自由度，讓我可以隨心所欲進行感興趣的實驗。安惠榮老師在每周一次的會議上，一次又一次的修正我的研究方向。於平博士手把手帶領我做實驗，鉅細靡遺的將他的專業知識、經驗傳授給我，為我找到研究的方向。他們是我能順利完成研究畢業的最大功臣，真的非常感激。實驗室人才濟濟，文小明博士對各種光學系統都有深厚了解，扮演了我最好的求救對象；院繼祖博士研究量子點多年，每每有相關問題就會向他請教；鄭信民博士和李弘賢博士熟悉半導體材料合成相關技術，和他們討論獲益良多。戴伯澤博士和我只短短相處 4 個月，但卻帶領我走入超快雷射領域，教導我其基本知識。期望這些給予我幫助的博士後們，能在未來找到一份心儀的研究工作。熱血的國晏、可愛的維尼，兩位學長常常陪我做實驗，老是麻煩你們我也很不好意思，還是只能一句感謝。高音頻昀睿、布丁狗賢真、帥氣黃婕、籃球姐 Fish，你們的陪伴讓實驗室的氣氛輕鬆自在，充滿了笑聲。安老師實驗室的誌彰、賈哥、小至、晏銘學長撐起了碩一時的會議，讓我愉快的度過碩一的歡樂時光。陪伴了我兩年的好夥伴們：美麗的紀瑩、誠懇的育昇、幽默的東東，和我一起度過修課、做實驗、會議上被責備的日子，謝謝，也祝福你們未來都有光明的前程。夏天火氣大的宇傑、重訓室魔人的厚升、安老師實驗室的珉澤、邦賢、修禾、可揚，實驗室就交給你們囉！希望你們的實驗也都能順利。當然，一定要感謝我的家人，這兩年是你們的支持和鼓勵，我才能完成我的碩士學位。在我鬧脾氣、耍任性時，你們的關懷和包容，現在回想起來真的很感動。最後，謹將這篇論文獻給我的父母，生養我、栽培我，是我心靈上和經濟上的支柱。謝謝你們。

## Table of Contents

<b>ABSTRACT</b> .....	I
<b>Acknowledgement</b> .....	IV
<b>Table of Contents</b> .....	V
<b>List of Tables</b> .....	VII
<b>List of Figures</b> .....	VIII
<b>Chapter 1 Introduction</b> .....	1
1-1 Semiconductor Quantum Dots .....	1
1-2 Motivation and literature review .....	3
1-3 Layout of thesis .....	9
<b>Chapter 2 Semiconductor Quantum Dots (QDs) and Organic molecules</b> .....	11
2-1 Quantum confinement in Semiconductor QDs .....	11
2-2 Structure properties of QDs.....	15
2-2.1 Surface of QDs .....	15
2-2.2 Shell passivation .....	17
2-3 Optical properties of QDs .....	19
2-4 Organic molecules .....	22
<b>Chapter 3 Experiment methods and Apparatus</b> .....	23
3-1 Transient absorption two color pump-probe measurement.....	23
3-1.1 Wavelength tunability and optical parametric amplifiers .	25
3-1.2 Experimental system of pump probe setup .....	28
3-2 Temperature dependent PL measurement.....	30
3-3 Sample preparing.....	33
<b>Chapter 4 Results and discussion</b> .....	35

4-1	Transient absorption .....	35
4-2	Steady-state fluorescence .....	39
4-3	Time resolved photoluminescence .....	43
4-4	Temperature dependent fluorescence .....	45
4-4-1	Fluorescence intensity .....	45
4-4-2	Energy gap variation .....	51
4-4-3	Band width of fluorescence .....	58
<b>Chapter 5 Recommendation for Further Work and Summary .....</b>		<b>62</b>
5-1	Electronic coupling in CdSe/CdS film .....	62
5-2	Summary .....	67
<b>References .....</b>		<b>70</b>





## List of Tables

Table 2-1. Showing the thiols under investigation with chemical formula and $pK_a$ . .....	22
Table 4-1. Show the double exponential function fitting parameters of Figure 4-2. The last row indicates the average decay lifetime. ....	38
Table 4-2. Shows the activation energy of QDs and with thiols extracted from fluorescence intensity fitting curve in figure 4-7. ....	50
Table 4-3. Fit parameters of the energy gap variation in QDs temperature dependent fluorescence measurement. It was fit using equation 4-6. ....	55
Table 4-4. Parameters used in the fit of the photoluminescence FWHM as a function of temperature by equation 4-7. ....	61
Table 5-1. The peak position and band width of pure QDs and DTT treated film in 4 different sizes with peak variation.....	64

## List of Figures

- Figure 1-1. Ou Chen *et al.* exhibit surface-functionalization-dependent excitonic absorption (a) Show that the transition energy and extinction coefficient of the  $E_2$  ( $2S_{h3/2}1S_e$ ) excitonic band of these nanocrystals can be strongly modified by their surface ligands as well as ligand-associated surface atomic arrangement. (b) Scheme of ligand effects on the electronic structure of a CdSe Nanocrystal [4]. .....2
- Figure 1-2. (a) Typical intensity time trace of CdSe/ZnS single-molecule QDs in TN buffer (upper panel) and in BME solution (lower panel). (b) Showing blinking behavior of single-molecule QDs reverse immediately as different solution delivered via a flow system [12]. .....4
- Figure 1-3. (a) **Effect of BME concentration and time on PL QYs of CdSe/ZnS QDs in pH-neutral conditions. QDs concentration is  $0.02 \mu M$ , with BME maximum 8 order higher than it [11].** .....5
- Figure 1-4. (a) **Upon addition of BME to a pH-neutral CdSe/ZnS NQD solution, the electron decay channel (fast 2 ps time constant) disappears. (b) Electron dynamics (up to 1 ns) are stable, with no return of the fast component over a day. (c) Time-resolved PL demonstrating the appearance over several hours of a new decay channel (1.6 ns dynamics). (d) PL intensity as a function of time and pH [11].**.....6
- Figure 1-5. **Steady-state emission spectrum for CdTe QDs at different**

pH values with different BME concentrations. The top two plots measured immediately after BME addition (A) at pH =7, (B) at pH = 9. The middle plots measured 4 hr incubation (C) at pH = 7, (D) at pH = 9. (E) QDs solubilized with BME compared with MPA QDs alone. (F) Samples deaerated with nitrogen flush [13] .....8

Figure 2-1. The bulk semiconductor has continuous conduction and valence energy bands separated by a fixed energy gap,  $E_g$ , whereas a semiconductor QDs is characterized by discrete atomic-like states and a QD size-dependent energy gap. The QD energy structures are shown for the model case of a two-band semiconductor, which has a single parabolic conduction band and a single parabolic valence band [19]. .....13

Figure 2-2. (a) Tunability of QDs nanocrystal. (b) Absorption and emission spectra of four CdSe/ZnS QDs. The blue line indicates the 488nm line of an argon ion laser, which can be used to efficiently excite all four types of QDs simultaneously. (c) The colorful PL spectrum [17, 18].....14

Figure 2-3. Showing the absorption and fluorescence spectra for electron-rich and cation-rich QDs situation [21]. .....16

Figure 2-4. Chemical structure of the CdSe semiconductor QDs (a) Bare CdSe QDs. (b) Core/shell QDs surrounded by ZnS or CdS. (c) Commercial CdSe/ZnS core/shell QDs further coated with polymer.....18

Figure 2-5. Schematic diagrams showing on/off light emission (blinking) in core/shell QDs (upper), and suppression of blinking in giant-shell and gradient alloy nanocrystals (lower).....21

Figure 2-6. Explain the blinking phenomena which is based on non-radiative Auger process. ....21

Figure 3-1. The simplified diagram to produce SHG and THG. The first nonlinear crystal produce SHG signal (400nm), and interacted with fundamental pulse in the second nonlinear crystal, reproducing THG signal (266nm). Dichroic mirrors are added to extract the specified frequency. ....25

Figure 3-2. Principle of OPA for extending the wavelengths through nonlinear interaction.....27

Figure 3-3. (a) Two color transient absorption pump-probe measurement setup. (b) The real photo of pump-probe setup. ....29

Figure 3-4. (a) Simply show the temperature dependent fluorescence experimental setup. (b) The real photo of the system.....32

Figure 3-5. (a) The absorption and (b) the fluorescence spectra of CdSe/ZnS core/shell QDs used in this study. The B1 feature (first absorption peak) is around 550nm and the PL peak is around 565nm at room temperature.....34

Figure 4-1. Transient absorption traces at the  $1P_e$  to  $1S_e$  for the CdSe/ZnS QDs in aqueous phase taken with different pump laser powers (shown in the figure).....37

Figure 4-2. Transient absorption spectra for CdSe/ZnS QDs with different short chain thiol-containing molecules at 24 hours aged.....	38
Figure 4-3. Steady-state fluorescence spectra of CdSe/ZnS QD with three different BME/QD molar concentration ratios vs. time. ....	41
Figure 4-4. Steady-state fluorescence spectra of CdSe/ZnS QD with three short chain thiols (5 order concentration ratios) vs. time. ....	42
Figure 4-5. Time-resolved photoluminescence spectra of CdSe/ZnS QD with three different BME/QD molar concentrations ratios and measured immediately and 24 hr incubation.....	44
Figure 4-6. The first plot is the temperature dependent fluorescence of pure QDs. The lower 6 figures show the PL with short chain thiols: BME, MPA, and NPM at 10 min and 24 hours at left and right side, respectively. ....	47
Figure 4-7. Arrhenius plot of fluorescence intensity for the edge-band of QDs with thiols. Evidently, pure QDs (black line) and BME, MPA, and NPM with 10 min and 24 hours (color line) incubation have large variation. ....	49
Figure 4-8. The energy gap extracted from PL curve fitted with single Gaussian as a function of temperature. All thiols: (a) BME (b) MPA (NPM) measured for immediately and 24 hr. incubation.....	53
Figure 4-9(a). Scheme of ligand induced internal electric fields or	

QCSE separates the electron and hole wave functions and therefore decreases the first exciton energy (red shift). .....56

Figure 4-9(b). Scheme of surface ligand induced hole transferred and trapped on the surface as covalent-type bonds was formed. Therefore, electron and hole separate and the energy gap red shift as case one.....57

Figure 4-10. FWHM bandwidth (dots) as a function of temperature and fit by equation 4-7 (solid lines) of QDs with (a) BME-capped (b) MPA-capped (c) NPM-capped. ....60

Figure 5-1. Showing the formula of dithiothreitol (DTT).....63

Figure 5-2. Absorbance of liquid (solid line) and solid (dotted line) for CdSe/CdS QDs ( $E_g = 2.35\text{eV}$ ) in citrate (black) and in DTT (blue).....64

Figure 5-3. The schematic diagram shows a dithiol molecule DTT connect to two QDs enhanced QDs coupling.....65

Figure 5-4. (a) Transient absorption spectra at low pump intensity  $\langle N_{\text{abs}} = 0.5 \rangle$  and various probe wavelengths near the  $1S_h - 1S_e$  transition for a QD / DTT film. (b) Contour plot of the same data for the QD / DTT film. The black line in (b) denotes the ground state absorption maximum. ....66

Figure 5-5. Schematic diagram of thiols and QD surface interaction. ....68

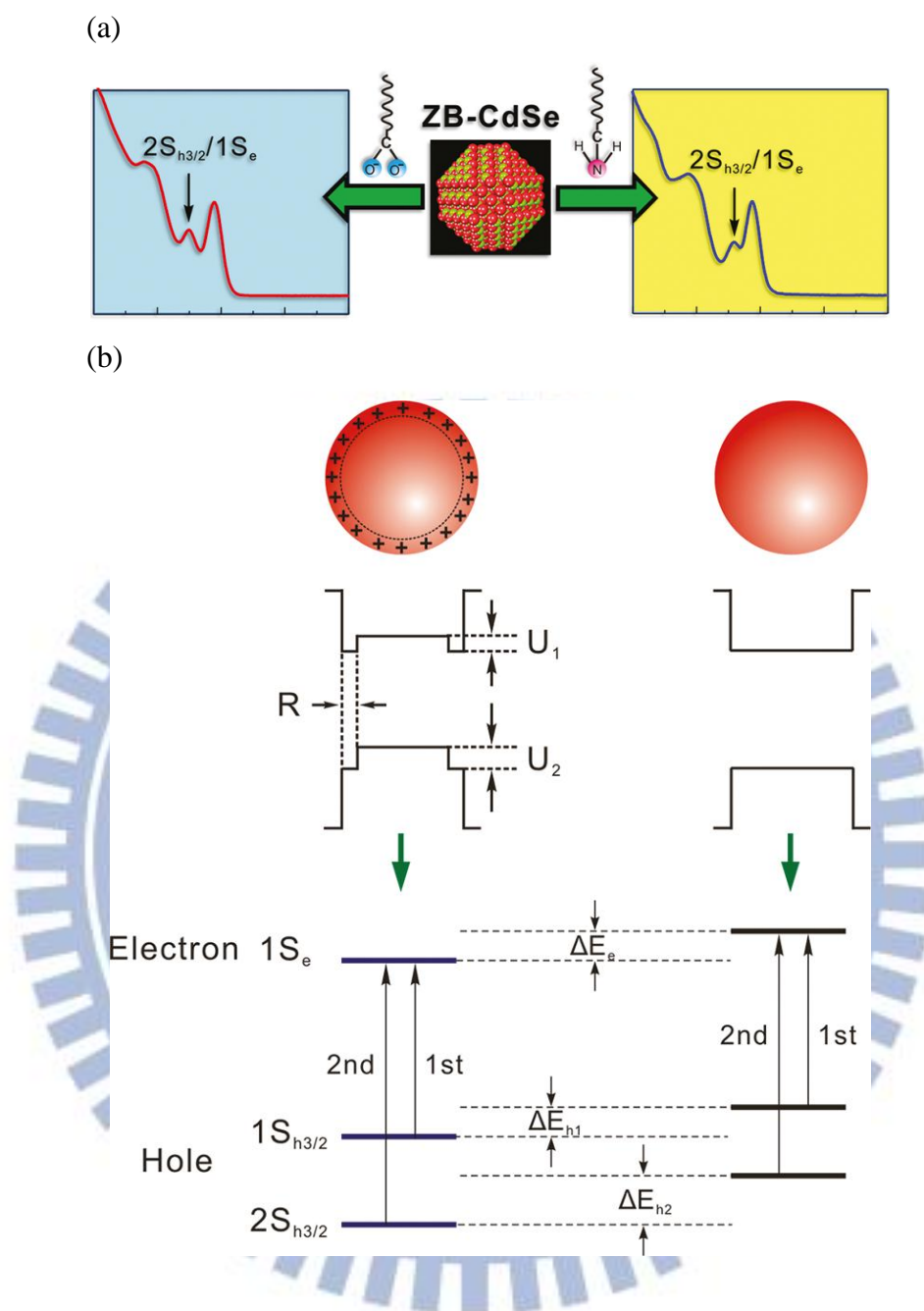
Figure 5-6. Schematic diagram of QDs surrounded by sulfur lone-pairs and suppress blinking by preventing core electrons eject to the defect sites of surface. ....69

# Chapter 1 Introduction

## 1-1 Semiconductor Quantum Dots

Colloidal semiconductor nanocrystals (NCs) or quantum dots (QDs) possess superior luminescence properties, high oscillator strength, photostability, broad absorption and narrow emission spectra, and thus attract a lot of research attention as promising materials for various application including bio-imaging, bio-labeling and coding, FRET-based sensors, and as for microscopy, nanophotonics, and optoelectronic devices [1]. A substantial amount of work has focused on the measurement of properties in CdSe/ZnS core shell QDs, primarily due to the relative ease in synthesizing sample (well developed for II-VI NCs) in the strong confinement regime ( $r < \alpha_B = 5.6\text{nm}$ ) with narrow size dispersion and increased absorption coefficient [2].

However, the restrict size of QDs cause large surface-to-volume ratio dictates their electronic and optical properties are dominated by the surface electronic structure, particularly band-gap electronic states [3]. Defects on the QDs surface such as unpassivated dangling bonds, adatoms, kinks, and vacancies often form shallow or deep trap states of electrons or holes make broad electronic states. These dominate their optical characteristics such as quantum yields (QY), photobleaching, blinking behaviors and Auger recombination. To date, a number of methods have been developed to passivate and control the surface of colloidal QDs. The surface modification can control the surface defects, micro-structural morphology and surface electronic density distribution for optimization of optical properties [4, 5]. Thus, an appropriate chemical treatment of the QD surface can have extensive application. For example, slowing down the electron cooling rate by capping ligands exchange is important for the solar cell application [6-9].

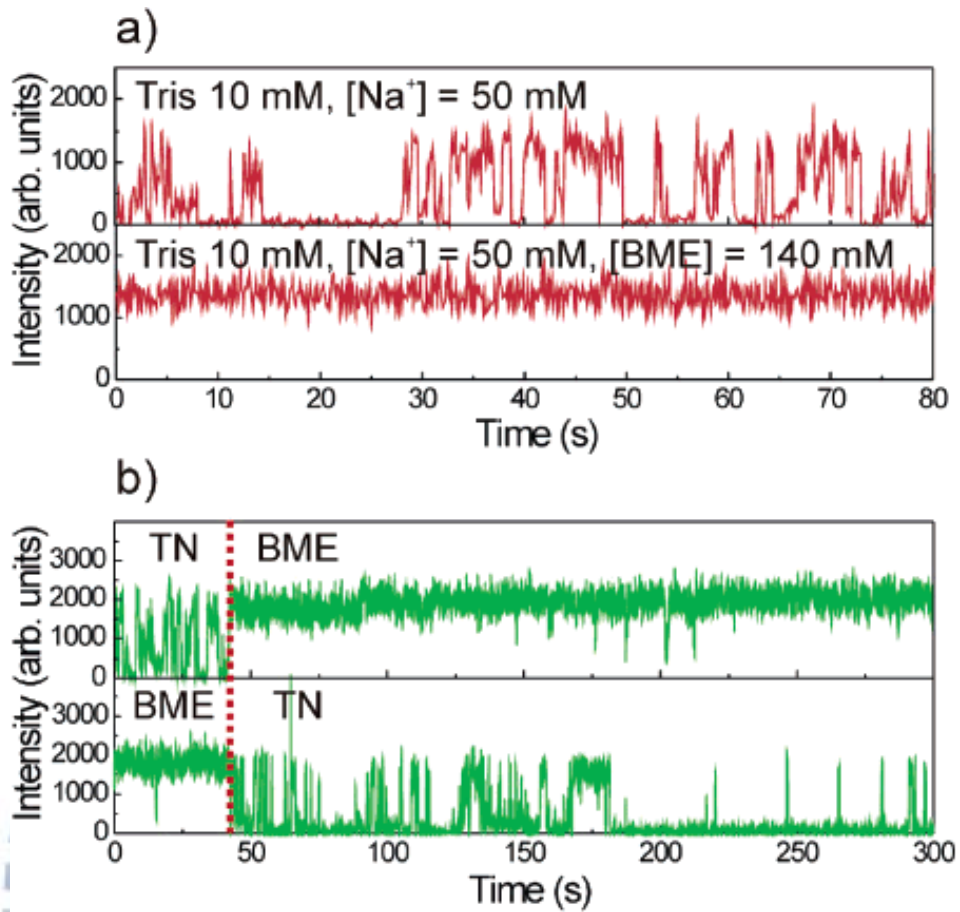


**Figure 1-1.** Ou Chen *et al.* exhibit surface-functionalization-dependent excitonic absorption (a) Show that the transition energy and extinction coefficient of the  $E_2$  ( $2S_{h3/2}1S_e$ ) excitonic band of these nanocrystals can be strongly modified by their surface ligands as well as ligand-associated surface atomic arrangement. (b) Scheme of ligand effects on the electronic structure of a CdSe Nanocrystal [4].



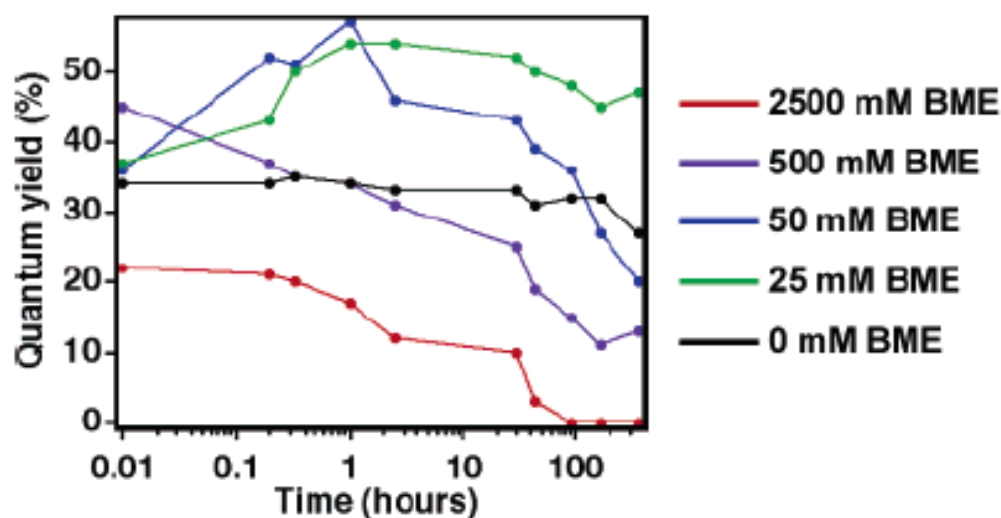
## 1-2 Motivation and literature review

Capping by the polymers or inorganic shell layers with higher band gap or molecule/atomic ligands exchange has been proved to be effective method for surface passivation and further confinement of charged carriers, therefore leading to a high luminescence efficiency [10, 11]. Thiol molecules are widely used in surface modification of QDs as well as metallic nanoparticles. Also, the optical properties of QDs are usually altered after the transform from thiol to thiolate whose chain lengths are relatively short. However, this process is complex and material dependent and has not been fully elucidated. Thiol-contained small molecules, beta-mercaptoethanol (BME), flush in pH-neutral aqueous solution can nearly completely suppress the blinking of single CdSe/ZnS QD was first discovered by Taekjip Ha and coworkers [12]. They have concluded these short chain thiols are highly dependent on the concentration, rather than number of thiol groups per molecule. It is surprising that the BME does not permanently change to show the quantum dot properties because the blinking behavior reappears immediately after replacing the buffer shown in Figure 1-2. The response attributed to thiol moiety, a potent electron donor, that could donate electrons to the surface electron traps renders them incapable of accepting electrons from the dot.



**Figure 1-2. (a) Typical intensity time trace of CdSe/ZnS single-molecule QDs in TN buffer (upper panel) and in BME solution (lower panel). (b) Showing blinking behavior of single-molecule QDs reverse immediately as different solution delivered via a flow system [12].**

Besides, Klimov *et al.* studied the PL efficiency and carrier dynamics as functions of thiol concentration, aging time, and pH to confirm the effect of thiols on QDs photophysics [11]. The continuous wave (CW) PL was used to characterize QYs shown in Figure 1-3, as a combination of time-resolved transient-absorption (TA) in  $1S_e$  and PL (*t*-PL) measurements, was used to monitor dynamics of photoexcited electrons and holes shown in Figure 1-4. Where the TA is only sensitive to changes in electron dynamics and *t*-PL is sensitive to both electron and hole dynamics. They found the thiol (in pH-neutral and acidic conditions) can provide surface passivation of QDs and enhance their quantum yields, while the thiolate (in basic conditions) plays as the hole traps and quench the PL. As Ha's work, it demonstrates strong concentration dependence.



**Figure 1-3. (a) Effect of BME concentration and time on PL QYs of CdSe/ZnS QDs in pH-neutral conditions. QDs concentration is  $0.02 \mu M$ , with BME maximum 8 order higher than it [11].**

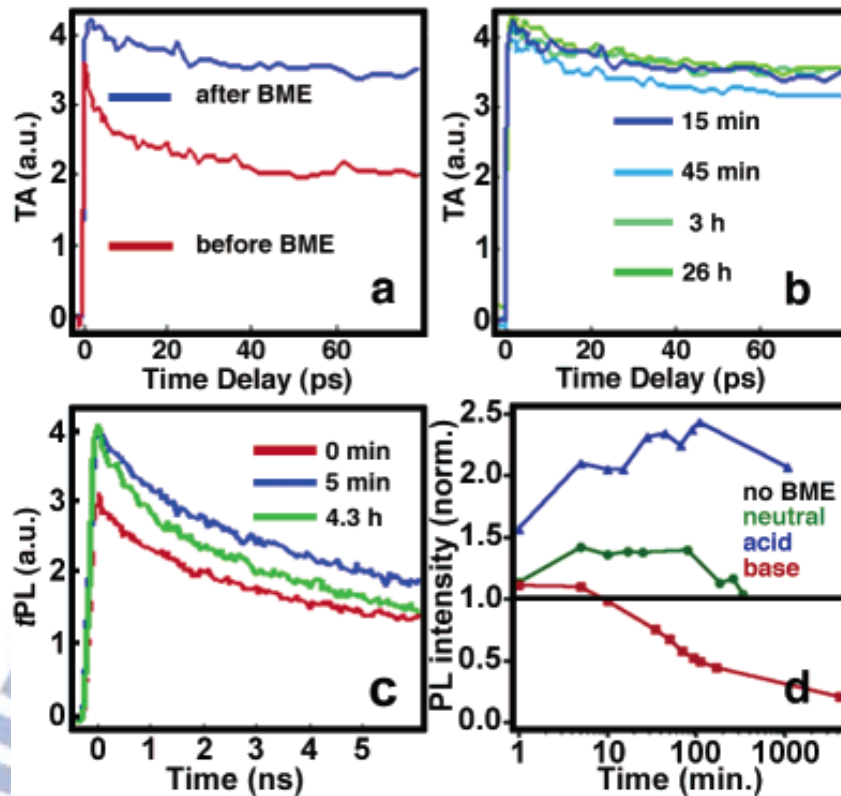
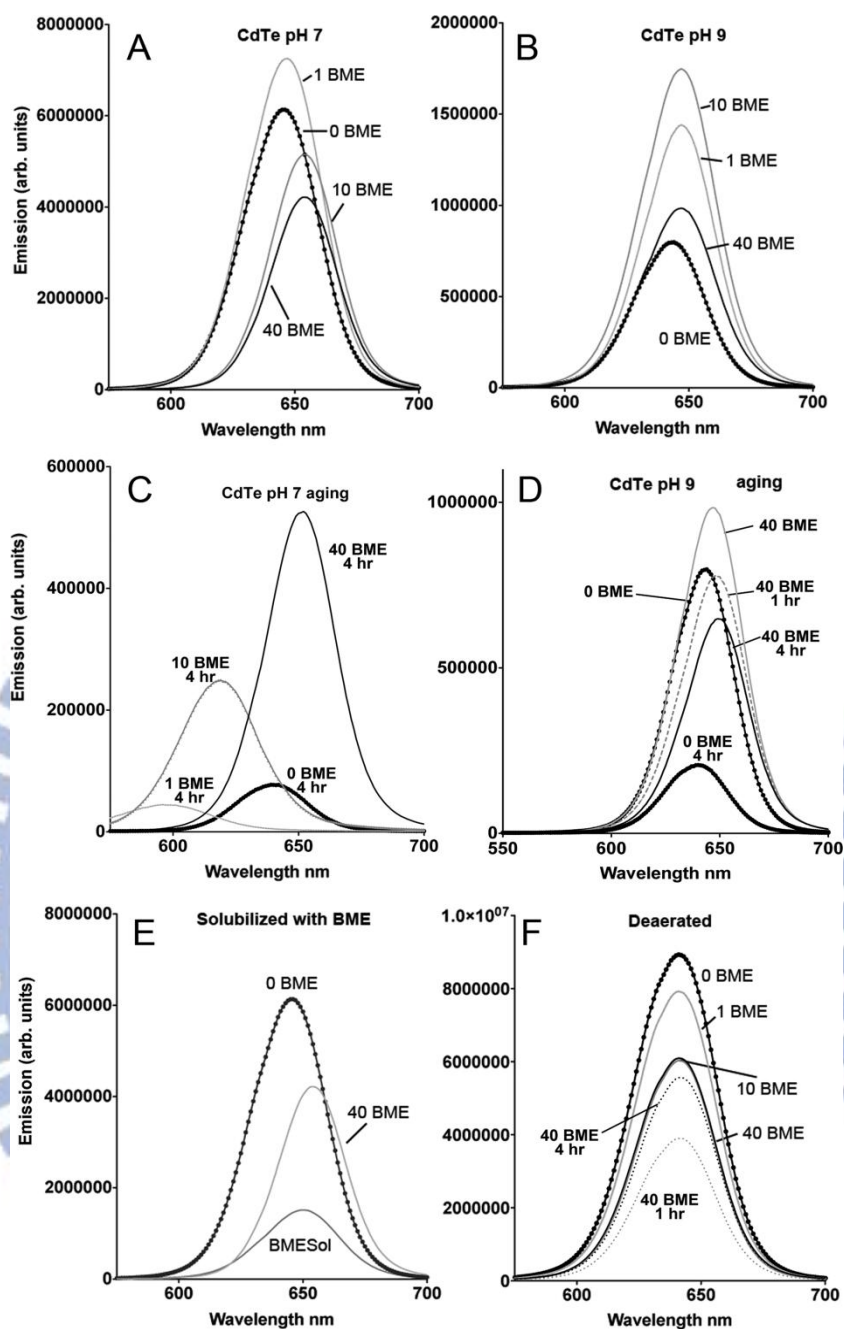


Figure 1-4. (a) Upon addition of BME to a pH-neutral CdSe/ZnS NQD solution, the electron decay channel (fast 2 ps time constant) disappears. (b) Electron dynamics (up to 1 ns) are stable, with no return of the fast component over a day. (c) Time-resolved PL demonstrating the appearance over several hours of a new decay channel (1.6 ns dynamics). (d) PL intensity as a function of time and pH [11].

Recently, the higher concentrations of BME will increase the radiative recombination lifetime in QDs due to elimination of oxygen in solution has been demonstrated by Nadeau *et al.* [13]. The luminescence lifetime decays were measured by time-correlated single photon counting (TCSPS) and fit to a model of radiative recombination and trapping. It confirms the BME antioxidant effects and the complicated processes involved concentration, pH, aging time, and QDs materials. Figure 1-5 shows the irregular fluorescence spectra at different pH values and BME concentrations. The relations of these factors need to be clarified.

In addition, Nelson *et al.* observe that the thiol molecule will create electronic traps on the PbS QDs surface and these trap states strongly depend on the chemical nature (e.g., anchoring groups, conjugation, and molecular length) of the molecule bonding to the QD surface [3]. These trap sites are mobile at the room temperature and the behavior also occurs in CdSe QDs by theoretical calculation [14]. The reversible formation of surface electronic trap states on thiolate-capped PbS QDs can be attributed to the mobility of surface capping molecules.



**Figure 1-5. Steady-state emission spectrum for CdTe QDs at different pH values with different BME concentrations. The top two plots measured immediately after BME addition (A) at pH =7, (B) at pH = 9. The middle plots measured 4 hr incubation (C) at pH = 7, (D) at pH = 9. (E) QDs solubilized with BME compared with MPA QDs alone. (F) Samples deaerated with nitrogen flush [13].**

### **1-3 Layout of thesis**

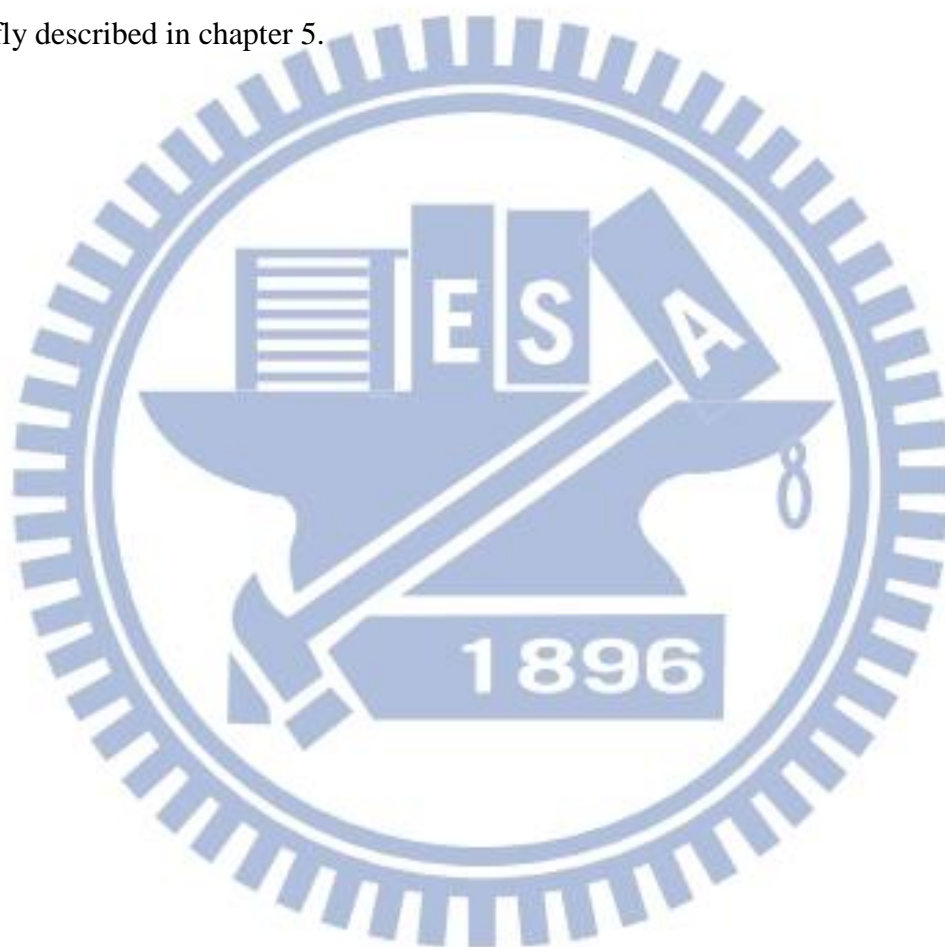
The surface-dependent optical properties of colloidal quantum dots have been extensively studied in the past two decades. This advance has led to the preparation of a variety of high-quality colloidal nanocrystals with composition of II-VI, III-VI, and IV-VI semiconductors. The CdSe/ZnS core/shell colloidal QDs under investigation were purchased from Invitrogen Canada Inc. To our best knowledge, the QDs were widely used in many single-particle experiments and the function of short chain thiol-containing molecules yet to be clarified. So far, there is no ensemble ultrafast spectroscopy and temperature dependent PL data combined to understand the effect of surface ligand on structure and optical properties of QDs. Ultrafast spectroscopy provides a suitable means to investigate dynamical processes. Temperature dependent fluorescence experiments further study the surface modification influence including band gap, surface trap site and activation energy.

In this study, we used QD sample with different thiol-containing molecules to examine the effect of QD surface-thiol interaction on defect sites immediately and long aging time (24 hours). The thesis is organized as follows. The first chapter is a briefly introduction to colloidal semiconductor quantum dots (QDs) and related research review carrying on the motivation of this study. Chapter 2 presents a basic knowledge of semiconductor quantum dots structures and optical properties. The thiol-containing short chain molecules used in this study were also depicted in this chapter.

The description of the measurement system including transient absorption pump-probe technique and temperature dependent system setup are described in Chapter 3. We discuss the fundamental principles and the detailed experimental setups and sample used in our experiments. Besides, the real photos of these experiment systems were also shown in this chapter.

In chapter 4 we provided the detailed experimental results and interpretation for

CdSe/ZnS core/shell quantum dots with short chain thiol molecules. We applied up-conversion photoluminescence and pump-probe transient absorption to detect the carrier dynamics on various time scales and discuss the physical meaning of the spectroscopy. The results were also confirmed by temperature dependent PL experiments. To identify the variety of thiol-molecules and QDs interaction, the steady state fluorescence vs. time was used. A summary and suggestions for future work were briefly described in chapter 5.





## Chapter 2 Semiconductor Quantum Dots (QDs) and Organic molecules

### 2-1 Quantum confinement in Semiconductor QDs

Usually, a natural length scale of electronic excitations in macroscopic, bulk semiconductors is given by the exciton Bohr radius,  $\alpha_B$ , which is determined by the strength of the electron-hole (e-h) Coulomb interaction. In ultrasmall NCs with sizes comparable with or smaller than  $\alpha_B$ , the dimensions of the nanoparticle but not the strength of the e-h Coulomb coupling define the spatial extent of the e-h pair state and hence the size of the NC exciton. The quantum dots (QDs), one of the central materials in nanoscience, is a semiconductor crystal with a physical size in the nano-order scale (~1-10 nm). The size of semiconductor QDs must be within the Bohr radius. It is often called an “artificial atom” because researchers can create nanostructures which yield properties similar to those of real atoms. The key feature of these inorganic materials is that they are physically intermediate between the limit of molecules and bulk solid. Being in this regime, the quantum dot is one of the canonical systems of nanoscience [15]. At nanoscale dimensions, the normal collective electronic properties of the solid become severely disordered and the electrons tend to follow “particle in a box” model, to account for approximated band structure. It represents a class of quasi-zero-dimensional objects in which carrier motion is restricted in all three directions. Bulk crystalline structure is preserved in NCs; however, due to three-dimensional (3D) quantum confinement NCs have atomic-like discrete energy spectra that are strongly size dependent [16]. If a QD is irradiated by light with photon energy ( $h\nu$ ) higher than bandgap ( $E_g$ ), an electron will be excited from valence band to conduction band. The bound state of the electron-hole pair is called an “exciton”, which can be used to study the relationship between the particle size and bandgap

energy of QDs. Equation 2-1 shows the dimension of particles decreases as the energy increases. By using the quantum confinement effects, it is possible to tune the energy bandgap. Therefore, the emission color could be changed over the whole visible range by varying the QD size, as shown in Figure 2-2(a) [17]. Moreover, the QD emission spectrum is symmetric in line shape and narrow in peak width. The absorption of QDs has an increase in probability at higher energies and a broadband and continuous absorption spectrum as presented in Figure 2-2 (b) [18].

$$E_{g,QD} = E_{g,b} + \left(\frac{\hbar^2}{8R^2}\right)\left(\frac{1}{m_e} + \frac{1}{m_h}\right) - \left(\frac{1.8e^2}{4\pi\epsilon_0\epsilon R}\right) \quad \text{Eq. (2-1)}$$

Where  $E_{g,QDs}$  and  $E_{g,b}$  are the bandgap energies of the bulk solid and quantum dot, respectively. R is the radius of QDs,  $m_e$  is the effective mass of the electron in the solid,  $e$  is elementary charge of the electron,  $\hbar$  is Planck's constant, the  $m_h$  is the effective mass of the hole in the solid, and  $\epsilon$  is the dielectric constant of the solid.

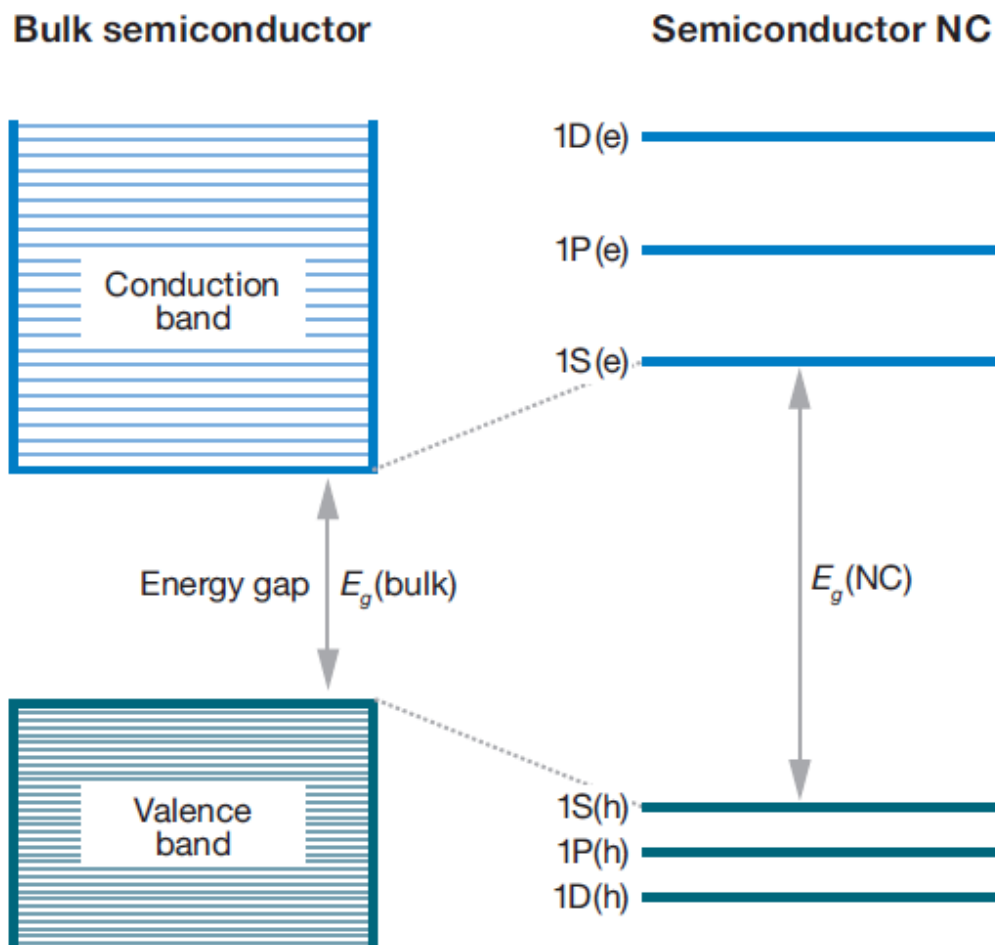
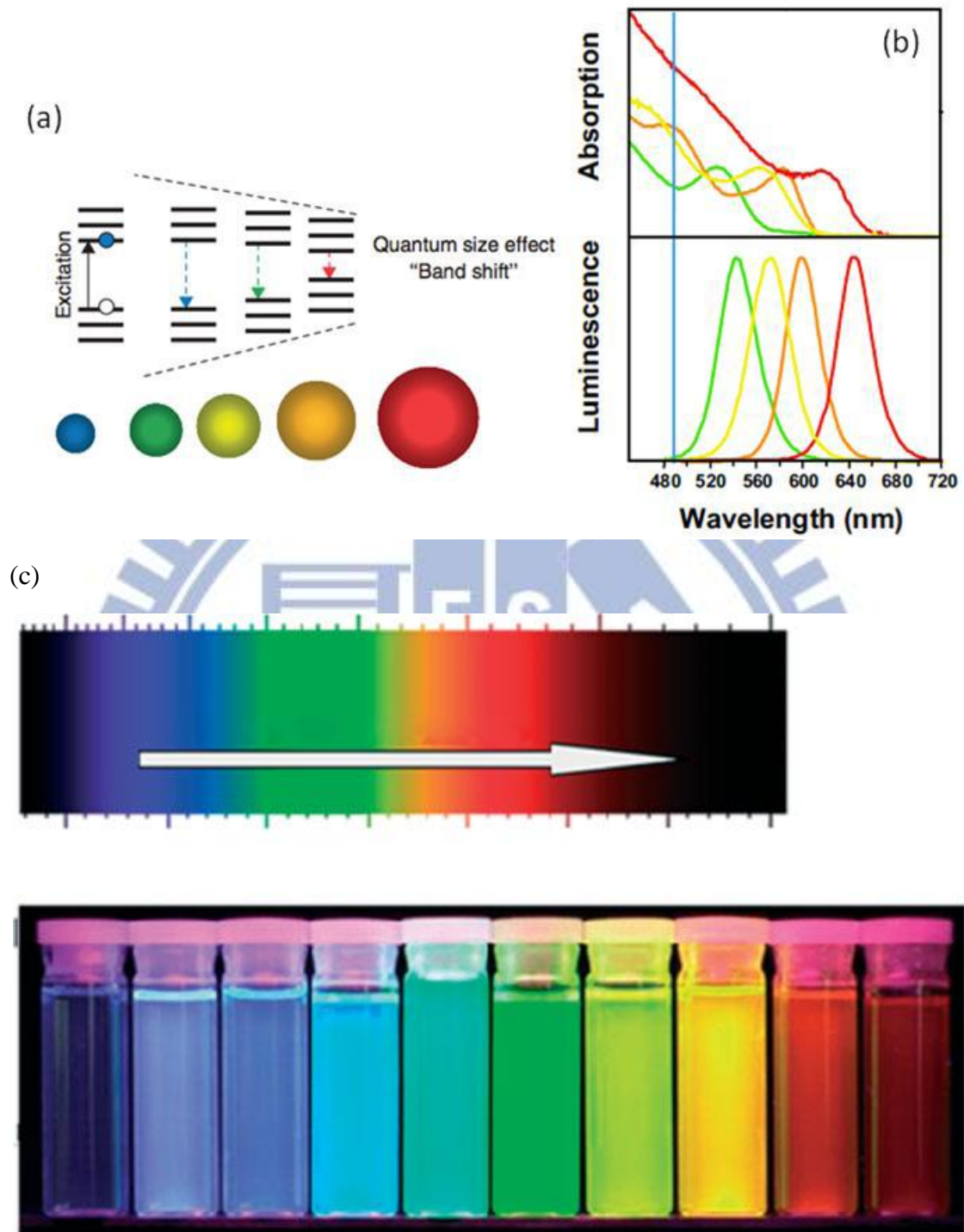


Figure 2-1. The bulk semiconductor has continuous conduction and valence energy bands separated by a fixed energy gap,  $E_g$ , whereas a semiconductor QDs is characterized by discrete atomic-like states and a QD size-dependent energy gap. The QD energy structures are shown for the model case of a two-band semiconductor, which has a single parabolic conduction band and a single parabolic valence band [19].



**Figure 2-2. (a) Tunability of QDs nanocrystal. (b) Absorption and emission spectra of four CdSe/ZnS QDs. The blue line indicates the 488nm line of an argon ion laser, which can be used to efficiently excite all four types of QDs simultaneously. (c) The colorful PL spectrum [17, 18].**

## 2-2 Structure properties of QDs

### 2-2.1 Surface of QDs

The dependence of optical properties on particle size is largely a result of the internal structure of the nanocrystal. However, as the crystal get much smaller like quantum dots, the number of atoms on the surface increases, which can also impact the optical properties. The atoms on the surface of a crystal facet are incompletely bonded within the crystal lattice, thus disrupting the crystalline periodicity and leaving one or more “dangling orbital” on each atom pointed outward from the crystal. If these surface energy states are within the QDs bandgap, they can trap charge carriers at the surface, thereby reducing the overlap between the electron and hole, increasing the probability of nonradiative decay events. In fact, most semiconductor QDs are suspended in solution and covered with organic ligands. Thereby, the dangling bonds on the exposed facets are “passivated” by bonding with atoms or molecules, minimizing intra bandgap surface states and reducing surface atomic reconstruction. For colloidal QDs suspensions, molecules with polar end groups and hydrophilic polymers could absorb to positively charged QDs by their negatively charged properties [20].

The surface trap state could significantly modulate the fluorescence. The colloidal QDs often show two fluorescence emission bands: one at the band edge and another at lower energy resulting from recombination at intra band gap defect sites on the surface. Figure 2-3 demonstrates the surface properties dependent fluorescence [21]. The existence of trap states of QDs may lead to low fluorescence quantum yield, broad fluorescence, and blinking because of charge recombination pathway. In addition, defects on the surface of QDs functioned as temporary surface traps for an electron or hole, which can result in nonradiative relaxation and reduce quantum yield [17].

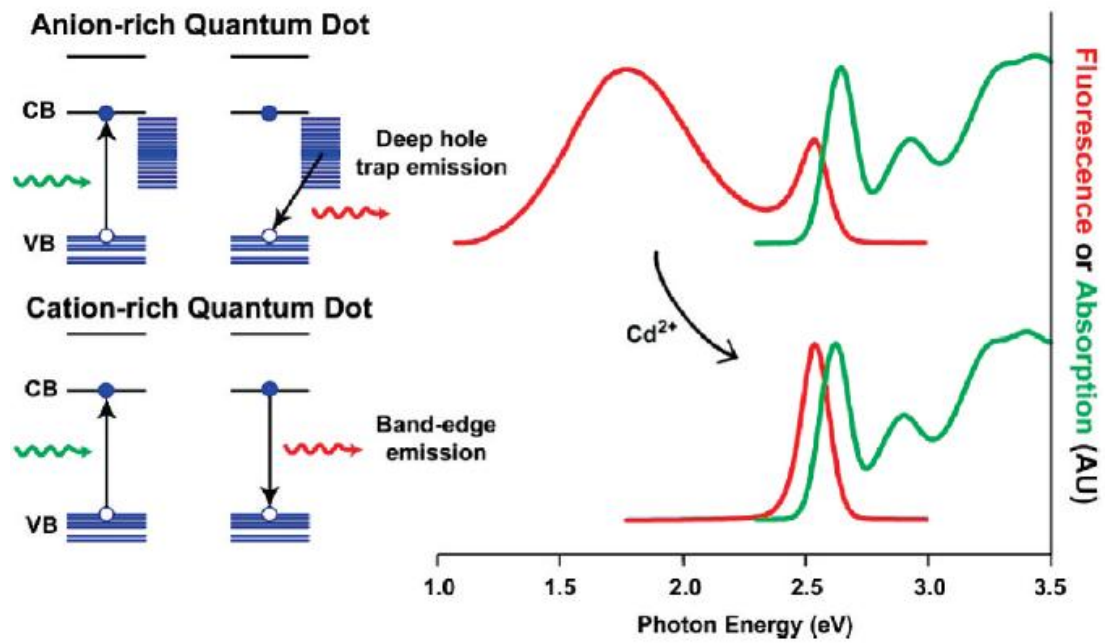
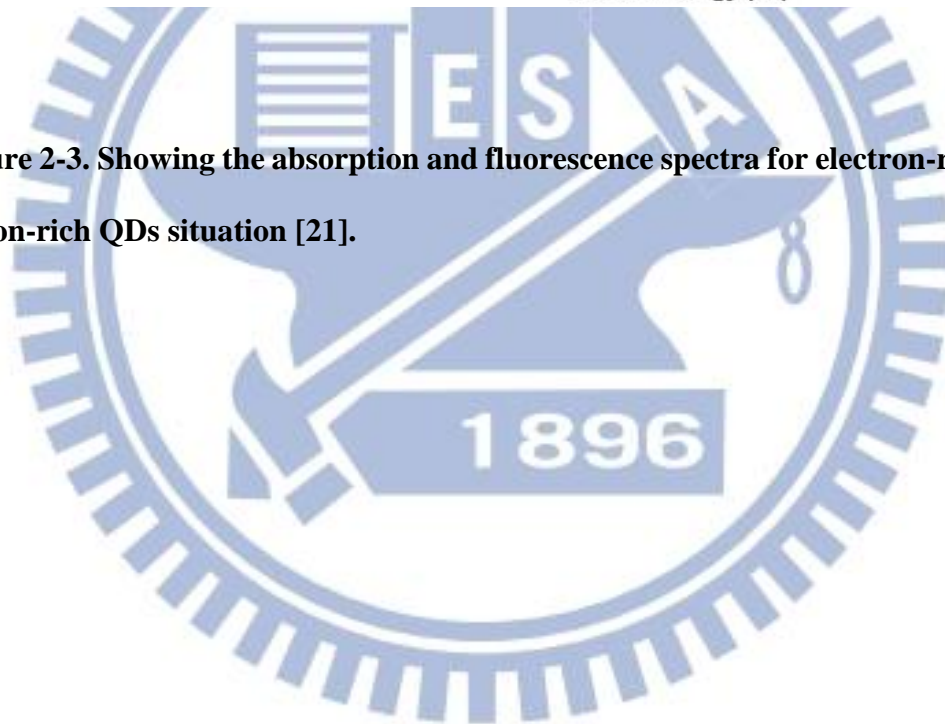


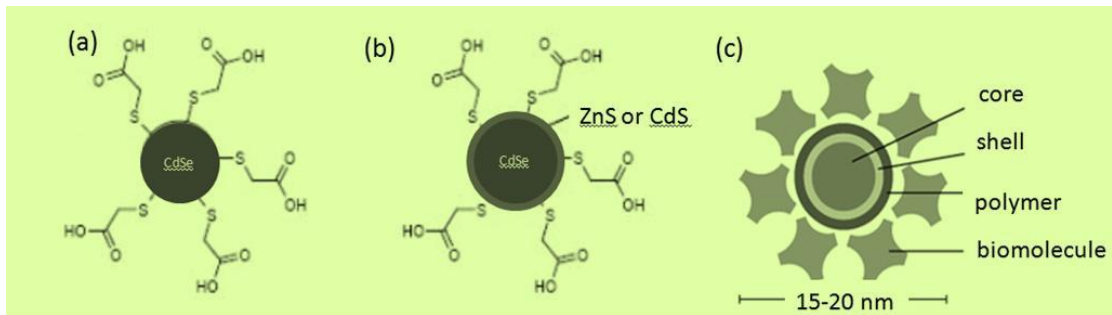
Figure 2-3. Showing the absorption and fluorescence spectra for electron-rich and cation-rich QDs situation [21].



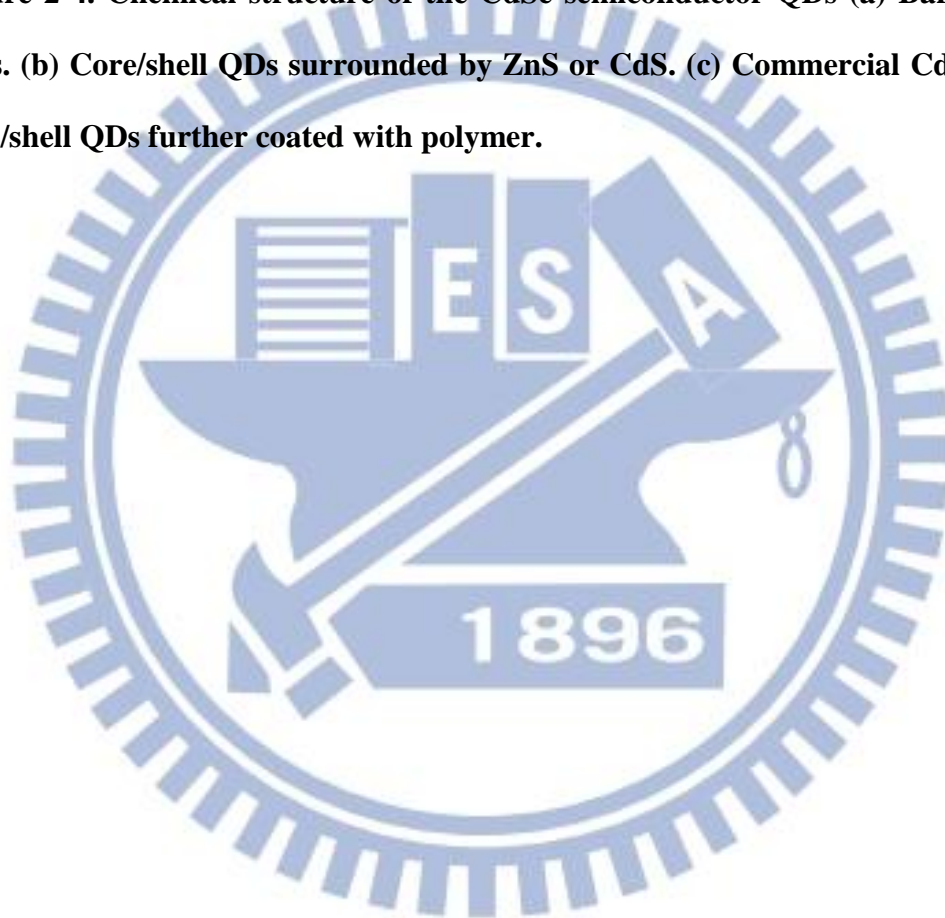
## 2-2.2 Shell passivation

For practical light-emitting applications, it is advantageous to coat semiconductor QDs with a shell in order to stabilize and maximize fluorescence. This not only passivates the surface bonds but also buries the semiconductor in a potential energy well, concentrating the charge carriers in the nanocrystal core, away from the surface [15, 17, 22]. Thereby, surface defect states and trap sites will have a diminished impact on the fluorescence efficiency and fewer environmental factors will influence the emission intensity. For colloid QDs, the normal progress of capping a shell to surround CdSe QDs is CdSe/CdS or CdSe/ZnS core/shell structure so that have efficient and stable fluorescence. Wider band gap CdS and ZnS shells not only electronically insulate the cores, but  $S^{2-}$  has a much lower oxidation potential than  $Se^{2-}$ , resulting in a higher threshold to photooxidative degradation and surface defect formation.

Recently, commercially available QDs are further coated with proprietary polymer and protein layers to render them biologically compatible. The compositions of three commonly used QDs are compared in Figure 2-4[[invitrogen.com](http://www.invitrogen.com)]. For bare QDs, solubilization is accomplished by self-assembly of an alkanethiol. The SH bonds connected to the semiconductor directly and the leaving carboxylate group is free to interact with aqueous solution. Core/shell QDs are overlaid with a 1-2nm thick layer as mentioned before. The solubilization is similar to bare QDs and the free carboxylates can be covalently bonded to proteins or other organic molecules of interest. Commercially available CdSe/ ZnS core/shell QDs further coated with polymers and the overall diameter is 2-to 3-fold. This kind of QDs is the investigation goal in this thesis.



**Figure 2-4. Chemical structure of the CdSe semiconductor QDs (a) Bare CdSe QDs. (b) Core/shell QDs surrounded by ZnS or CdS. (c) Commercial CdSe/ZnS core/shell QDs further coated with polymer.**





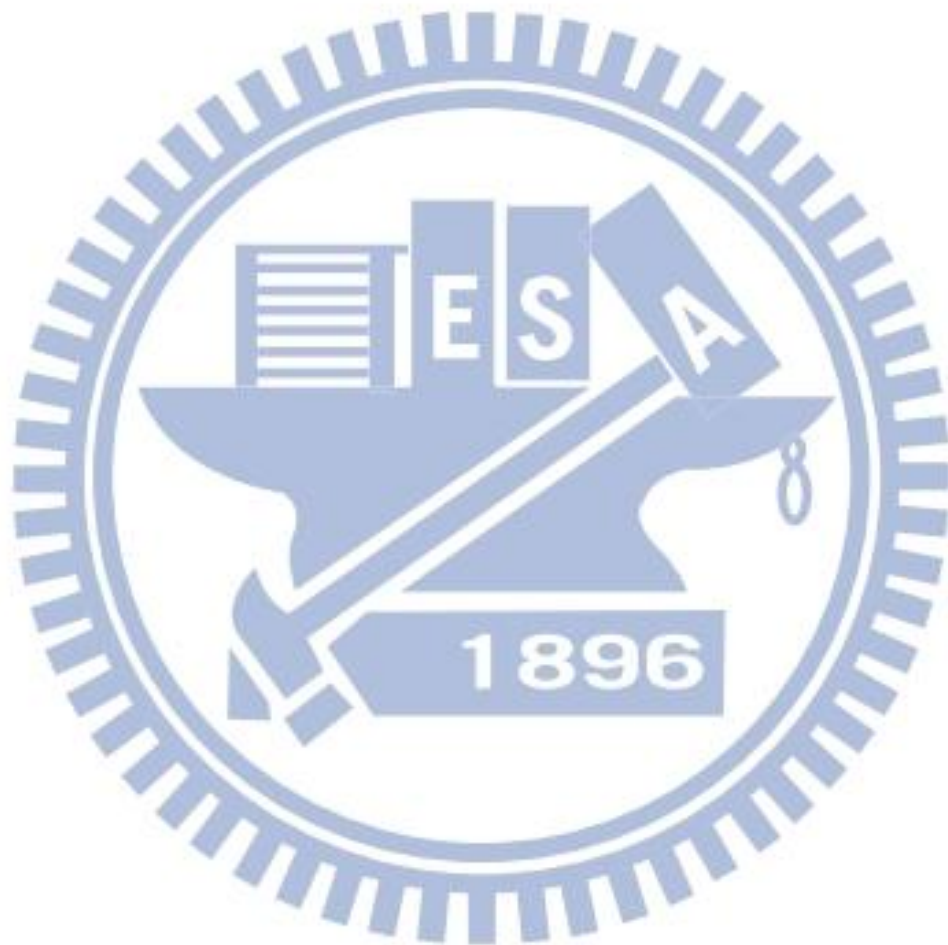
## 2-3 Optical properties of QDs

We have already mentioned lots of these advantages of semiconductor QDs, many of these applications suffer from yet another common property of QDs: intermittent fluorescence known as blinking [23]. This phenomenon is observed as the turning “on” and “off” of fluorescence emission under continuous excitation of QDs. The distribution of “on” and “off” duration has been found to follow inverse power law statistics and various models have been suggested to explain the mechanism of QD blinking [24-28]. Although the exact mechanism underlying this behavior is not yet entirely clear, there is a consensus regarding the effect of charge on the emission state of QDs [22].

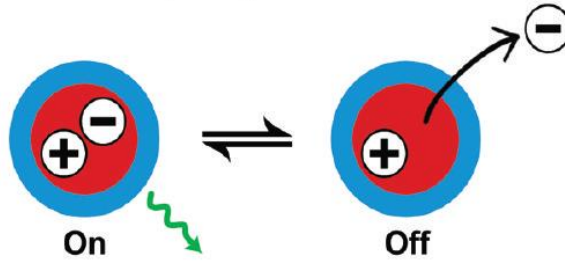
A canonical picture for describing QDs blinking phenomena is based on the Auger model, whereby fluorescence intermittency is caused by fluctuations in net charge inside or around the QDs [17, 23, 27]. Specifically, if photoexcitation results in an electron-hole pair, called neutral light state (or so called “on” state), there is a finite probability of either the electron or hole migrating to traps at the surface, leaving a delocalized charge in the nanocrystal core. Subsequent photoexcitation of a second electron-hole pair in the charged dot leads to transient trion formation, which can decay via nonradiative Auger processes much faster than the intrinsic radiative rate. The dark state (or called “off”) is generally attributed to the formation of such situation [29, 30]. This results in a transient photophysical state of low quantum yield, that can recover (i.e., “blink”) by reentry of charge from the trap state into the nanocrystal [31]. Such fluorescence blinking behavior depends on a variety of experimental conditions such as the thickness of the passivating inorganic shell, excitation intensity, and temperature [32, 33].

Thus, the existence of photoluminescence ‘on’ and ‘off’ periods significantly limits the number of photons that can be detected in a given time period and also makes

the photon arrival times from a single nanocrystal highly unpredictable. Blinking can also reduce the brightness in ensemble imaging via signal saturation [12]. Several reports have shown a correlation between the ensemble quantum yield and number of dark particles, with highly efficient batches showing fewer dark particles and a high probability of bright states for blinking particles [34, 35].



Conventional (Core)Shell Quantum Dots



“Giant Shell”  
Reduced Blinking

Alloyed Shell  
Nonblinking

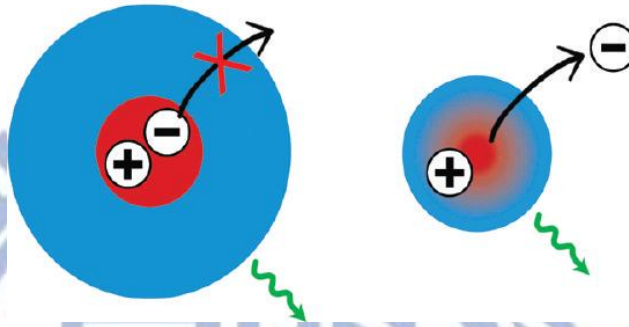


Figure 2-5. Schematic diagrams showing on/off light emission (blinking) in core/shell QDs (upper), and suppression of blinking in giant-shell and gradient alloy nanocrystals (lower).

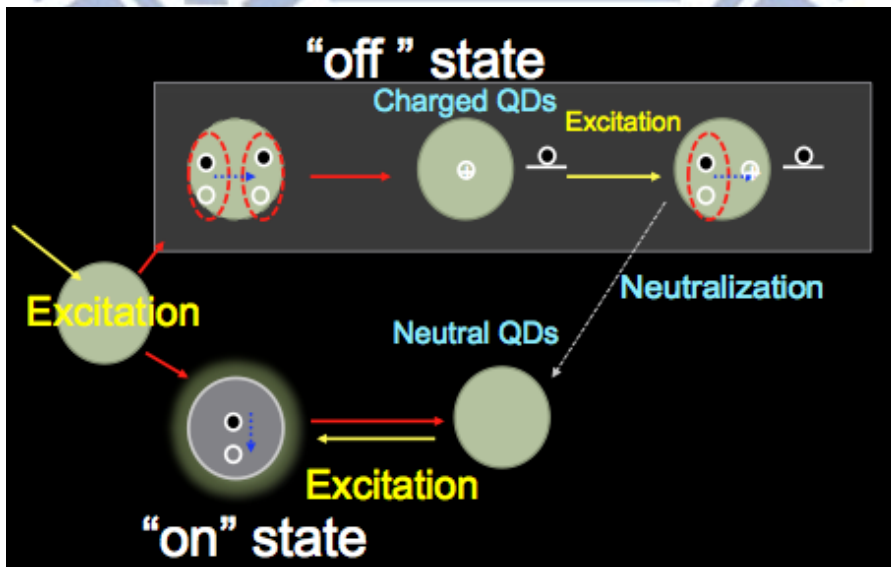

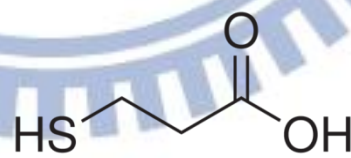



Figure 2-6. Explain the blinking phenomena which is based on non-radiative Auger process.

## 2-4 Organic molecules

Organic molecules have been proved to play a significant role for the properties of the inorganic semiconductor QDs, and thiol-containing short chain molecules could suppress blinking behavior of single QDs. Here we choose some organic molecules accord with our experiments. That are  $\beta$ -Mercaptoethanol(BME), 3-Mercaptopropionic acid (MPA), and 1-propanethiol(NPM). Where BME has been studied for a long time, and it will be a good bridge to other research. MPA and NPM are similar to BME, only with different functional group. Table 2-1 shows the chemical formula and  $pK_a$  of these thiols. It should be noted the  $pK_a$  here indicated the ability of thiol group dissociate to thiolate form.

**Table 2-1. Showing the thiols under investigation with chemical formula and  $pK_a$ .**

	Chemical formula	$pK_a$
$\beta$ -Mercaptoethanol (BME)		9.7
3-Mercaptopropionic acid (MPA)		10.3
1-propanethiol(NPM)		10.7

## Chapter 3 Experiment methods and Apparatus

### 3-1 Transient absorption two color pump-probe measurement

In Semiconductor QDs, some physical mechanisms influence the photoinduced carrier dynamics. Several measurements have been used to investigate it. However, femtosecond laser pump-probe system has been shown to be the most powerful tool to read the temporal and spectral dynamics of the carriers. The laser pulse width can achieve femtoseconds, and it's short enough to measure scattering or relaxation processes in QDs. The semiconductor QDs under investigation is excited by the pump pulse, the charge carriers will transit from valence band to conduction band, then relax back to valance band through various relaxation processes. Another weaker laser pulse, called probe pulse, will reach the sample with suitably delayed respect to the pump pulse by introducing an optical delay in its path. The probe pulse laser detected the transient photo-absorption (TA) signal in a continuous time domain.

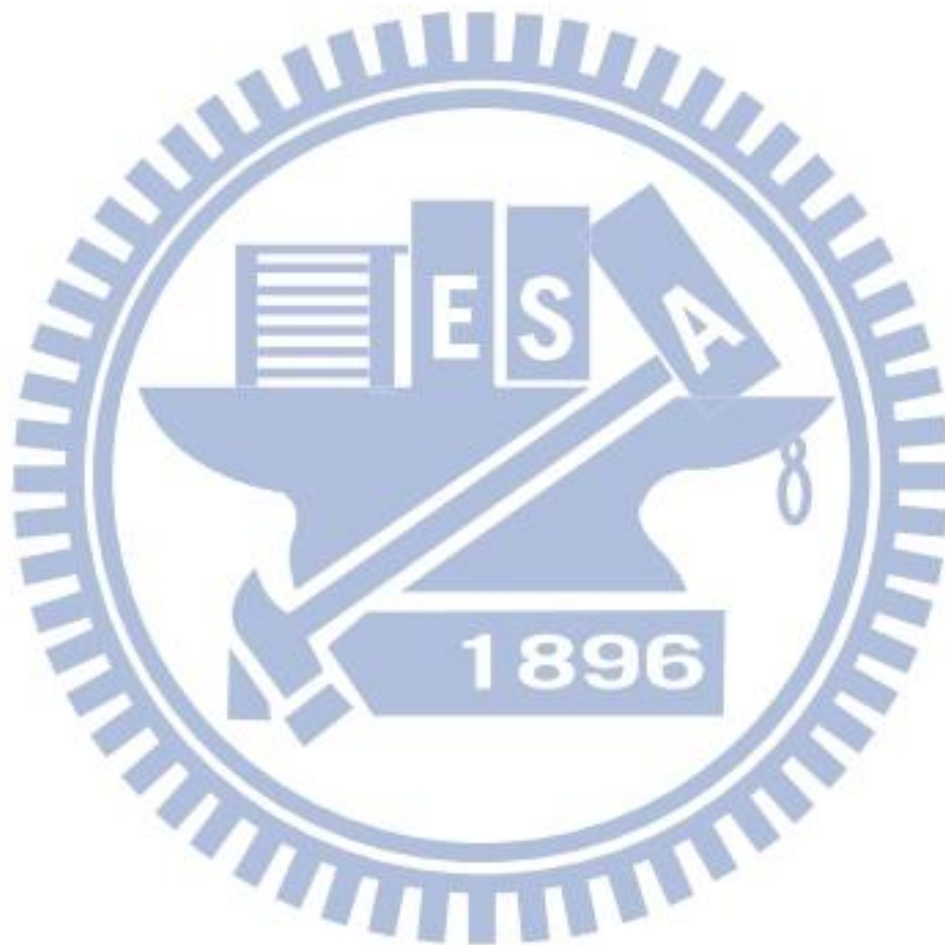
Normally, the probe power is much weaker than the pump power, and the spot size on the sample is smaller than the pump to ensure measuring a uniform photoexcited density. The data is expressed in the form of the normalized differential transmission given by  $\Delta T / T_0$

$$\frac{\Delta T}{T} = \frac{T(t) - T_0}{T_0} \quad \text{Eq. (3-1)}$$

Where  $\Delta T(t) = T(t) - T_0$  is the change in transmission induced by the pump, T and  $T_0$  are the transmission of the probe in the presence and absence of the pump, respectively. The resulting signal is proportional to the sum of electron and hole distributions at the probe photon energy and therefore has the potential to separately measure electron and hole dynamics in semiconductor QDs. This contrasts with other ultrafast spectroscopic

techniques such as TRPL, in which the measured signal is proportional to the product of the electron and hole distributions, preventing separate measurements of electron and hole dynamics [2].

In order to obtain a flexible system, a non-degenerate (pump and probe at different wavelengths) measurement over a broad spectral range is required. Below we will show the experiment setup in detail.



### 3-1.1 Wavelength tunability and optical parametric amplifiers

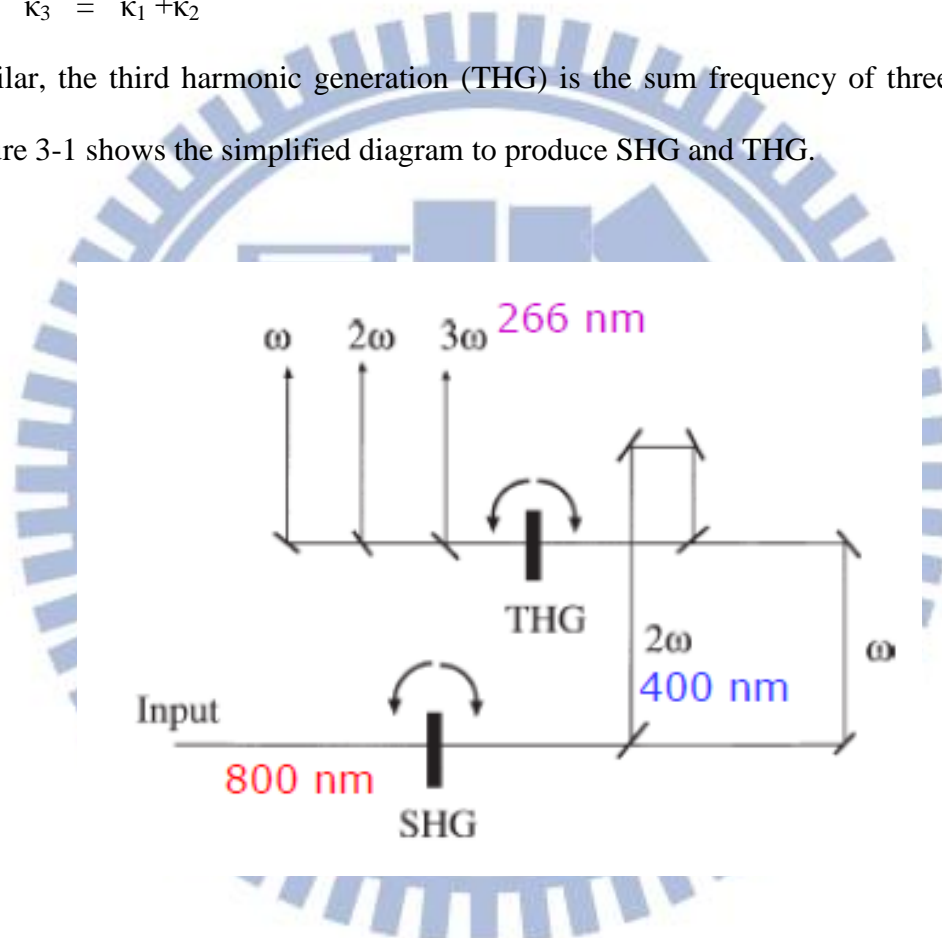
Second harmonic generation (SHG) is a simple nonlinear laser technique to generate sum frequencies. Two laser pulse have interactions in nonlinear crystals such as BBO ( $\beta$ -barium borate), LBO (lithium triborate), KTP (KTiOPO<sub>4</sub>). Fulfilled the phase-matching condition, as equation shows below:

$$\omega_3 = \omega_1 + \omega_2 \quad (\omega_3 = \omega_1 - \omega_2)$$

$$\kappa_3 = \kappa_1 + \kappa_2$$

Similar, the third harmonic generation (THG) is the sum frequency of three pulses.

Figure 3-1 shows the simplified diagram to produce SHG and THG.



**Figure 3-1. The simplified diagram to produce SHG and THG. The first nonlinear crystal produce SHG signal (400nm), and interacted with fundamental pulse in the second nonlinear crystal, reproducing THG signal (266nm). Dichroic mirrors are added to extract the specified frequency.**

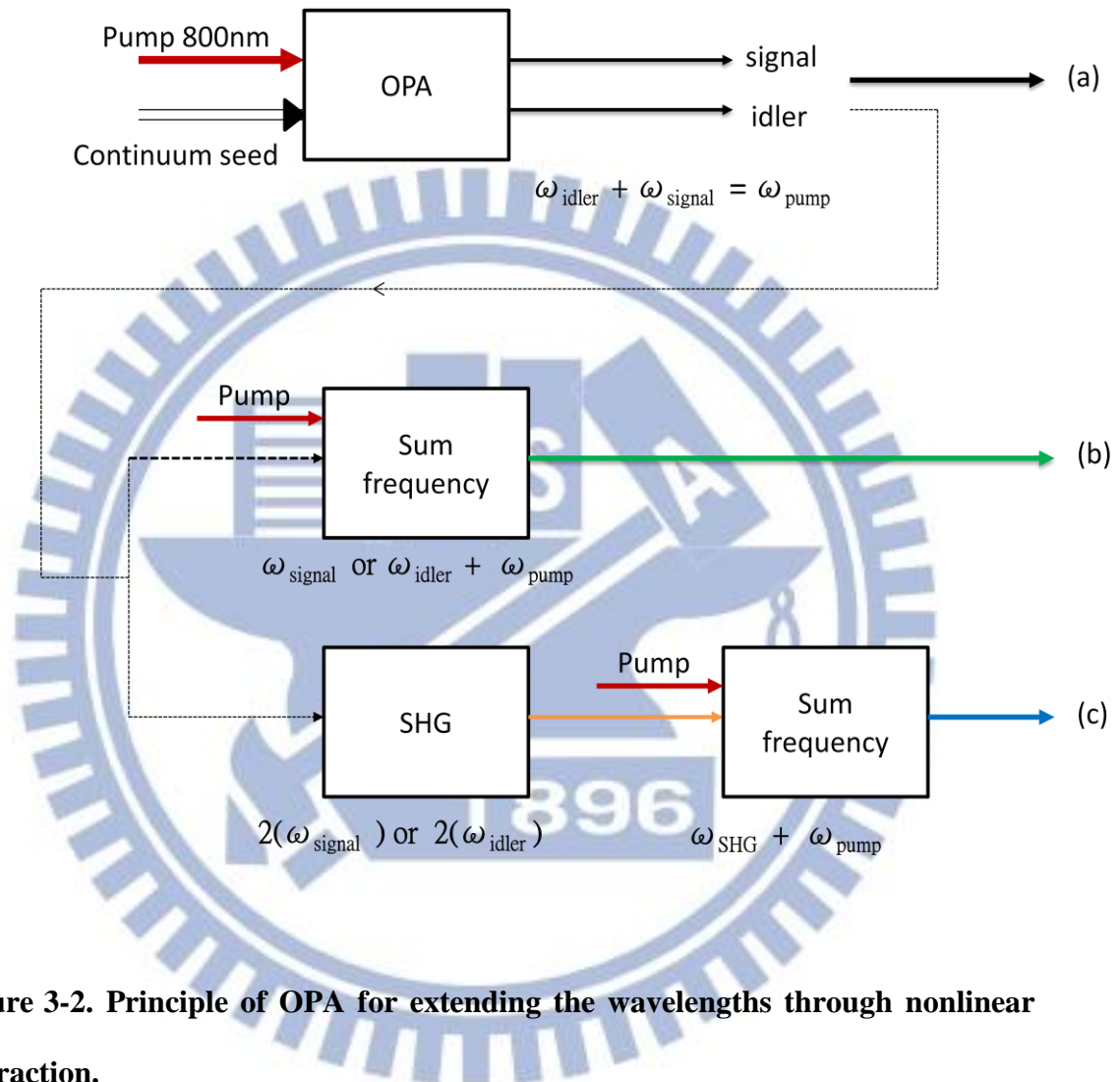
In our system, a laser pulse pass (800nm) through focal lens focused on nonlinear b-barium borate (BBO) crystal with a large  $\chi^{(2)}$ , generating a double frequency pulse (400nm). It's take 40-50% conversion efficiency for 800 nm to 400 nm. Usually, we choose a sufficiently thin nonlinear crystal to reduce the group velocity dispersion (1mm). This 400nm pulse laser acted as the pump beam.

Optical parameter amplifiers (OPA), as illustrated in Figure 3-2, show the principle of the OPA for extending the wavelengths. Firstly, 800 nm ultrashort pulses can be easily obtained as the fundamental, and 400 nm and 266 nm pulses can be obtained by nonlinear second harmonic generation (SHG 400 nm) and third harmonic generation (THG 266 nm), respectively. A white-light continuum pulse with ultrashort width is generated as a seed by a focused pulse (800 nm) passing through a sapphire plate. Pumped by the fundamental, the OPA oscillates and emits both signal and idler beams with perpendicular polarizations and tunable near infrared wavelengths. Then the signal and idler can mix with the fundamental to generate visible wavelengths through sum frequency generation (SFG). The second harmonic of the signal or idler can also mix with the fundamental to generate visible and ultraviolet output. Thus, the OPA system, through nonlinear techniques, can produce ultrashort pulses with wavelengths extending from the near infrared to the ultraviolet.

This wide range pulse laser is used as the probe beam source for its flexible wavelength. We use a commercial OPA system pumped by the Ti:sapphire regenerative amplifier laser (TOPAS-C, Spectra Physics). It is a two stage parametric amplifier of white-light continuum. Briefly, there are some blocks including: pump beam delivery and splitting optics, white light continuum generator, a pre-amplifier or first amplification stage, a signal beam expander-collimator and a power amplifier or second amplification stage. We use a personal computer to control translation stage and rotation stages so that allow for a fast and precise optimization of positions of certain



optics when tuning the output wavelength of TOPAS-C. We use 550nm laser because of the B1 of QDs under investigation.



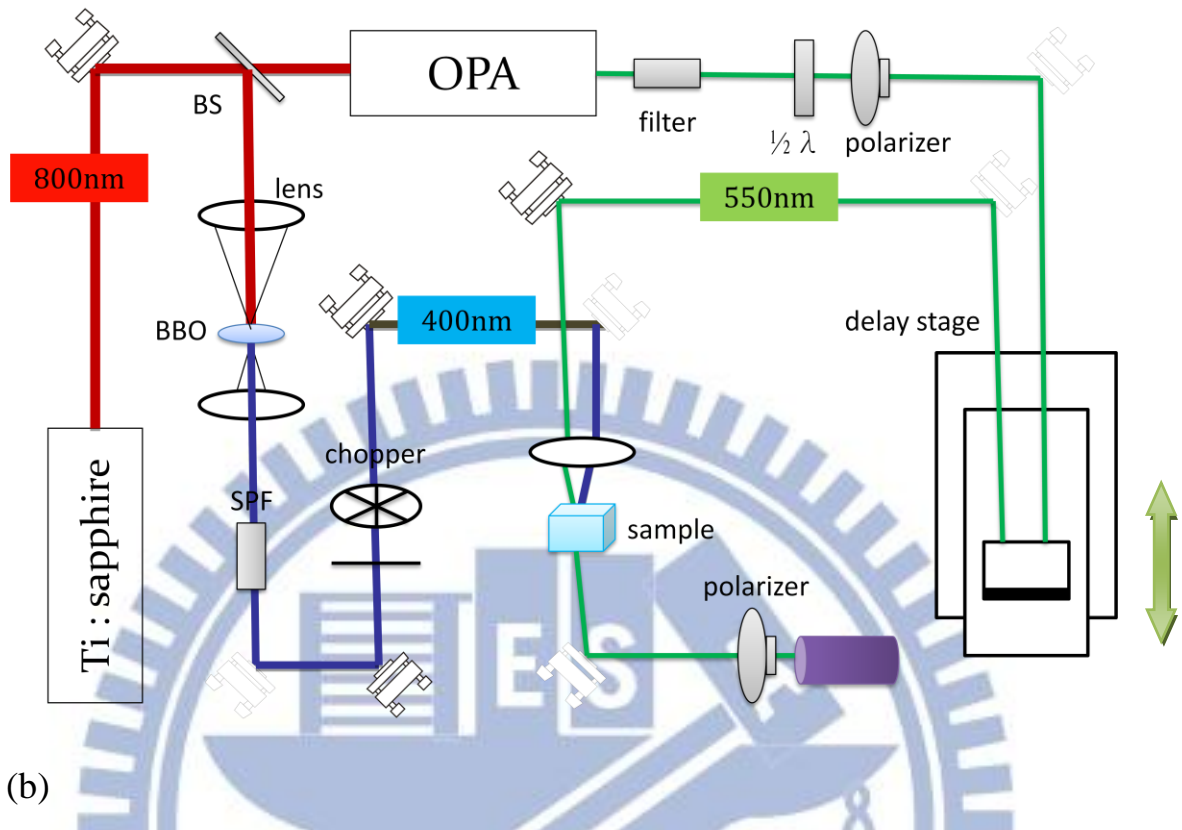
**Figure 3-2. Principle of OPA for extending the wavelengths through nonlinear interaction.**

### 3-1.2 Experimental system of pump probe setup

The transient absorption (TA) pump probe system setup is shown in Figure 3-3. It is based on a Ti:Sapphire amplified laser (Spitfire, Spectra Physics) with maximum output about 1mJ, 1kHz repetition rate, and central wavelength of 800nm. The output of the laser was split by a 90-10 beamsplitter, with the higher power portion transmitted into OPA as probe beam and lower power portion being frequency doubled in a 1mm BBO crystal as pump beam. The pump beam was modulated at 100Hz by an optical chirp. To avoid coherent interference and isolate two pulses, the calcite polarizer and half-wave plate pair is added to two pulses ensuring the polarizations of pump and probe beam are perpendicular to each other. The pump and probe beams were made collinear and focused at the sample with convex lens. We monitored the absorption signal with a silicon photodiode module (New focus 2001), the output of which was fed into a lock-in amplifier (Stanford Research Systems, SR830).

The intensities of the pump and probe beams were controlled by a combination of neutral density filters, polarizers, and half-wave plates. The ratio of the pump probe power is about 60:1. The relative delay between the pump and beams was controlled with a stepper motor-driven translation stage. Pump beam size is about 110 $\mu$ m/diameter after SHG with confocal lenses. The time resolution of our instrument is estimated to be 0.2ps (Gaussian FWHM). This is broader than the transform-limited pulse width of the Ti:Sapphire oscillator, mainly due to dispersion through the focusing objective [36, 37].

(a)



(b)

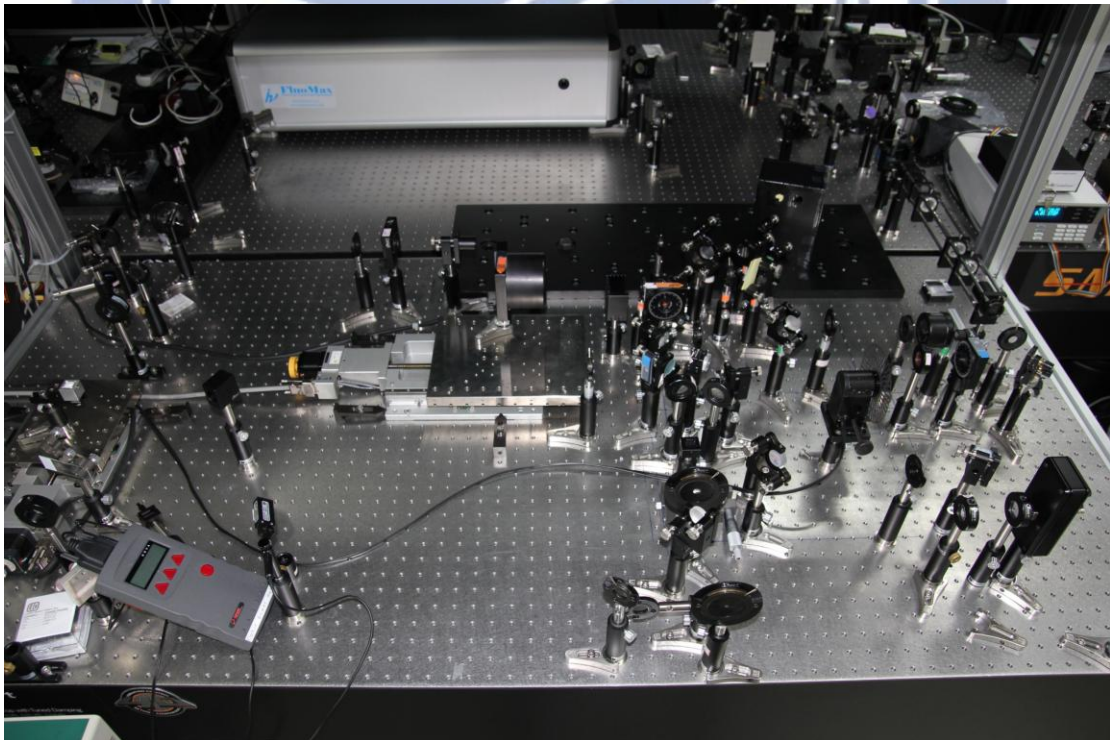


Figure 3-3. (a) Two color transient absorption pump-probe measurement setup.

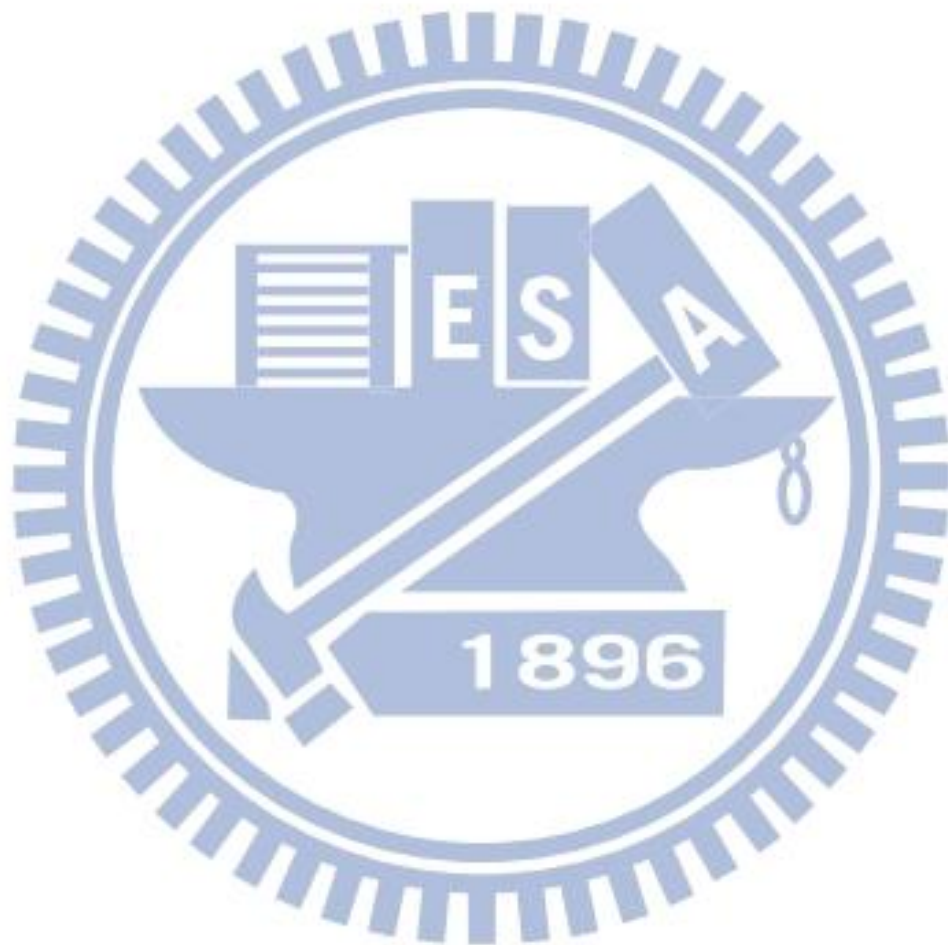
(b) The real photo of pump-probe setup.

### 3-2 Temperature dependent PL measurement

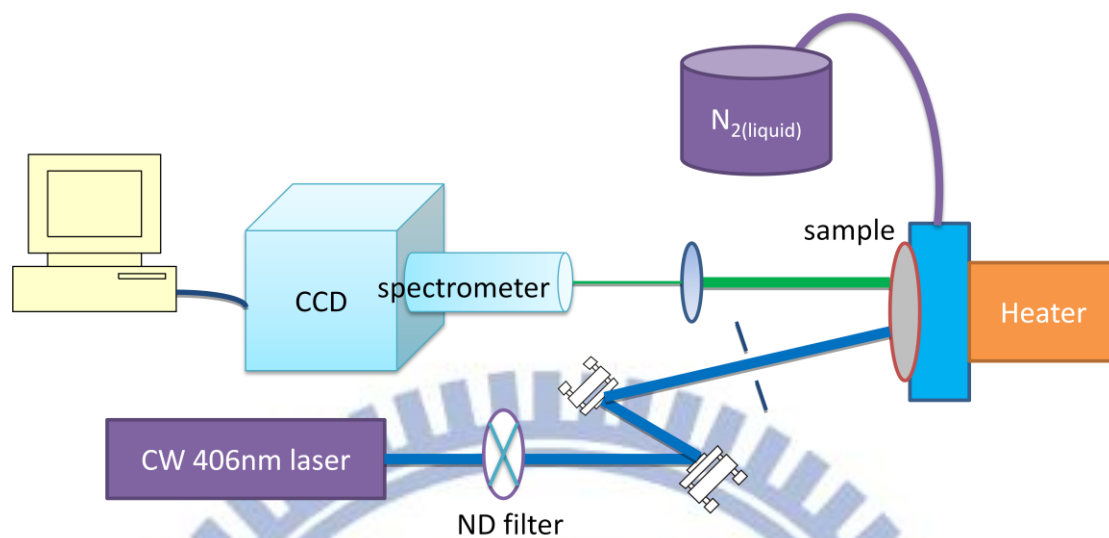
A detailed study of the QDs photophysics with a particular attention to nonradiative processes is not only interesting for fundamental physics, but it is also relevant to the exploitation of nanocrystals in practical applications. To date, several relaxation processes have been proposed to explain the photophysics of CdSe QDs, including the thermally activated exciton transition from dark to bright states and carriers surface localization in trap states [38]. As the result, a key aspect for understanding the fluorescence behavior is through studies of the radiative and non-radiative processes, which govern the temporal decay and the quantum yield of the fluorescence. Such investigation can be obtained through examination of the temperature dependence of fluorescence. It has been shown that at room temperature the main nonradiative process in CdSe/ZnS core/shell QDs is thermal escape, assisted by *multiple* longitudinal optical (LO) phonons absorption, while at low temperature evidence for carrier trapping at surface defects was found [39]. Despite these results, the role and the chemical origin of the surface defect states in the radiative and nonradiative relaxation in nanocrystals has not been clarified completely [40, 41].

The temperature dependent experimental setup was shown as Figure 3-4. A 406 nm CW laser with a power of 50 mW was used as an excitation source, and was attenuated using a neutral density filter with an optical density of 1.5 in order to avoid extra irradiation effects during the measurements. The excitation beam was spatially limited by an iris and unfocused. The excitation density on the surface is estimated to be  $50\text{mW}/\text{cm}^2$ . Fluorescence was collected into a MicroHR spectrometer (HORIBA Jobin Yvon) with a 1200 per mm grating and recorded by a cooled CCD (Synapse<sup>TM</sup> CCD). The spectral resolution of the system is around 0.5 nm. The sample was installed in a cryostat (ST500) in vacuum with controllable temperature between 77 and 450 K when using liquid nitrogen. For each sample, we perform PL

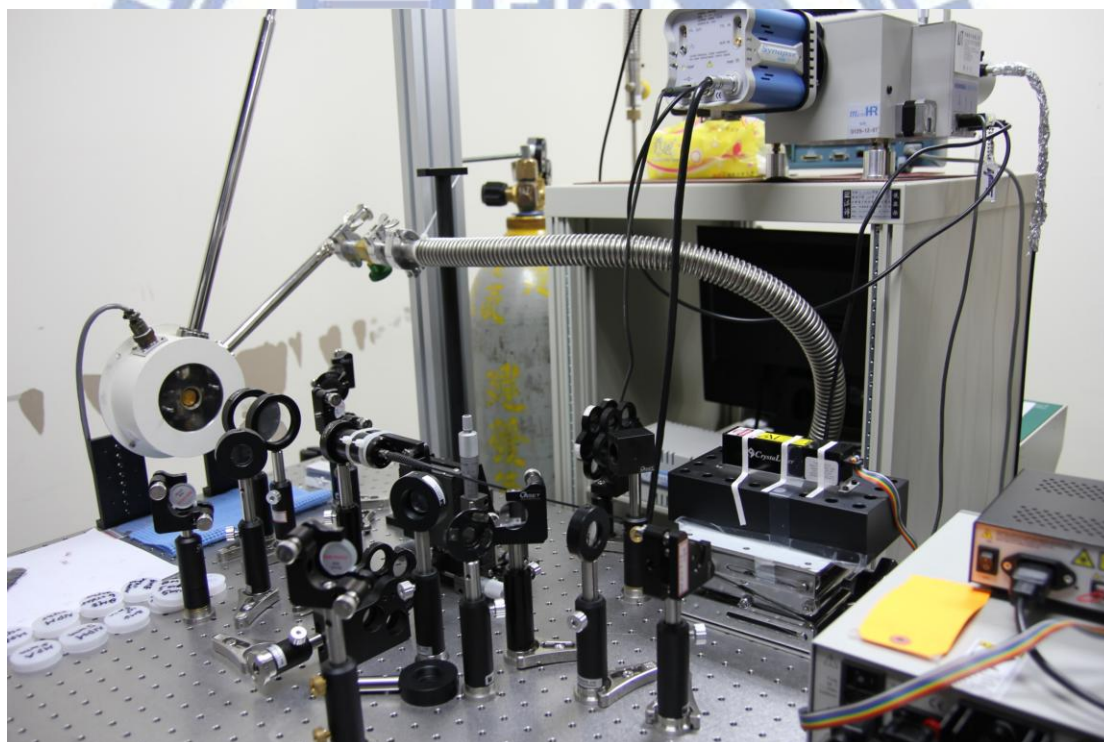
measurements in the temperature range from 77K to 300K (room temperature) in steps of 20K.



(a)



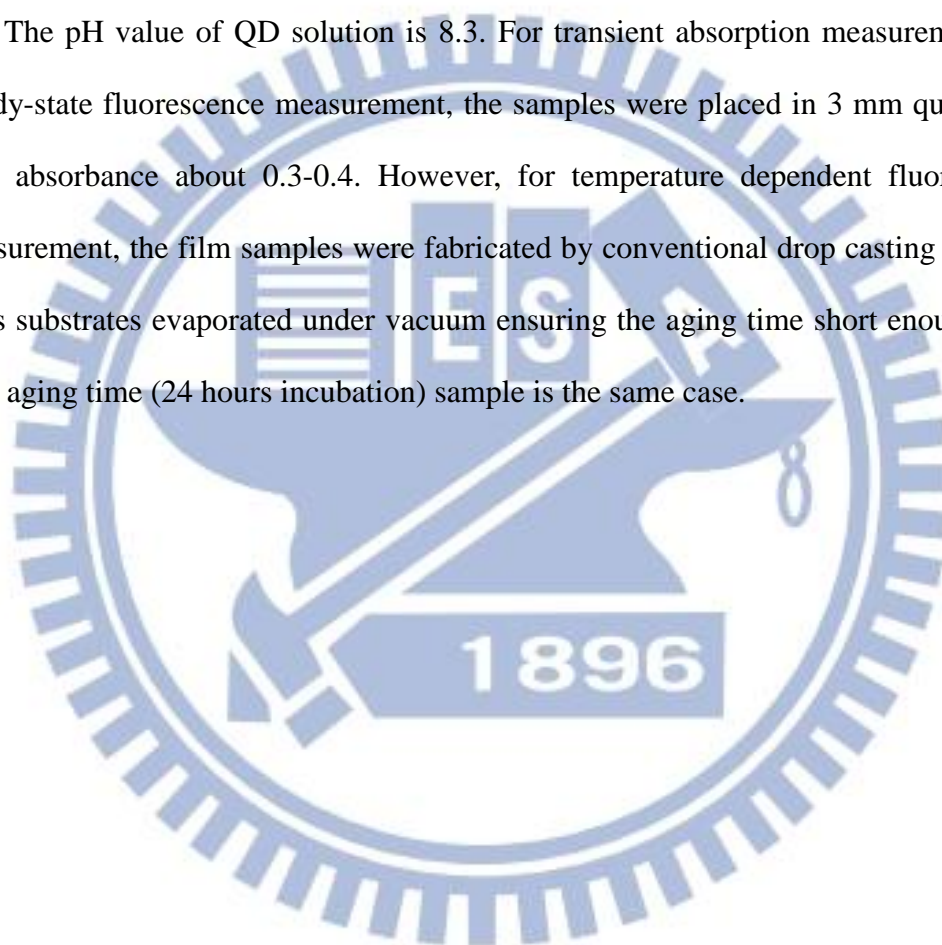
(b)

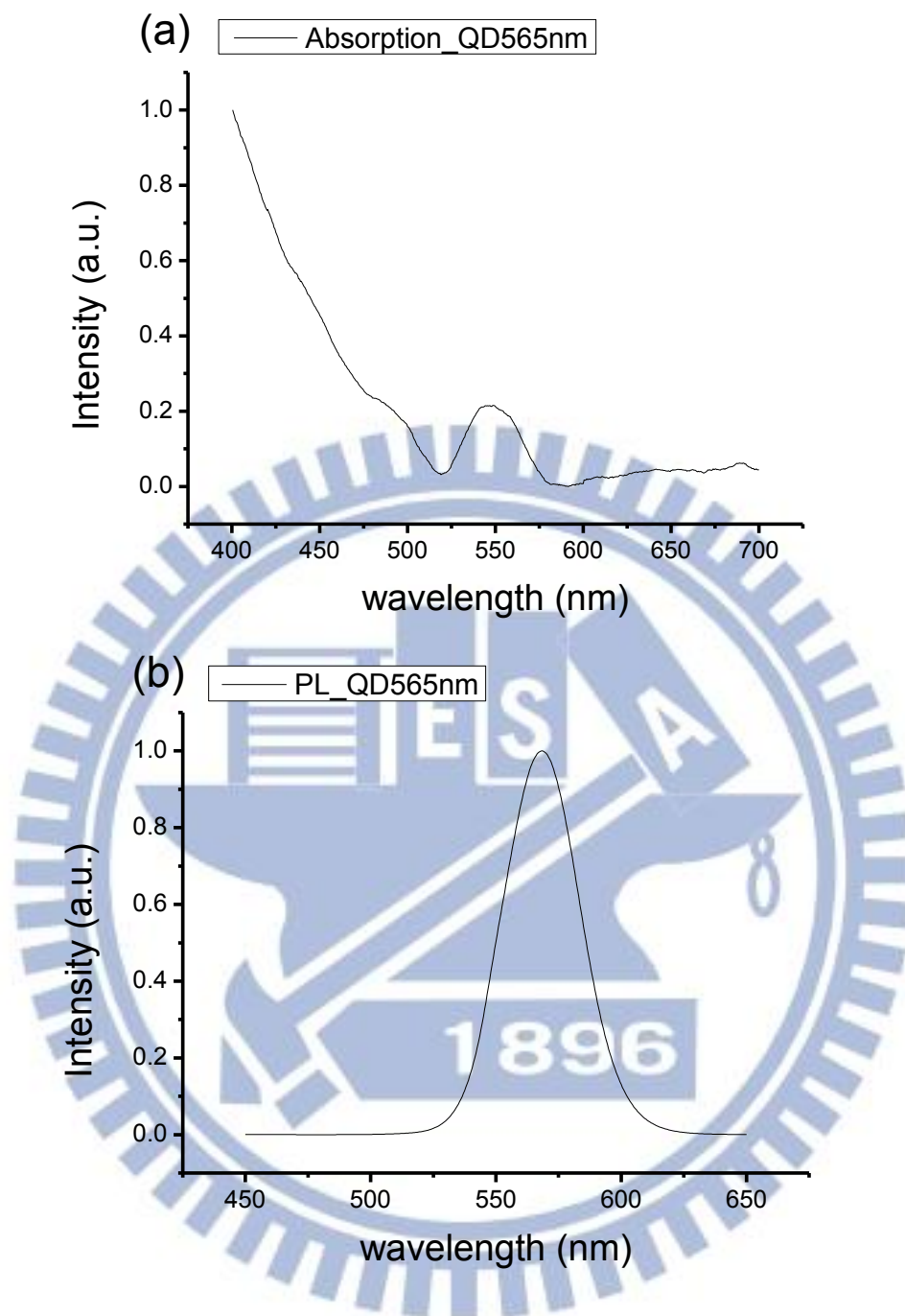


**Figure 3-4. (a) Simply show the temperature dependent fluorescence experimental setup. (b) The real photo of the system.**

### 3-3 Sample preparing

The CdSe/Zns core/shell QDs with polymer layer surrounded was purchased from Invitrogen Canada Inc. The Absorption and fluorescence spectra of QDs show in Figure 3-4. The short chain thiols including  $\beta$ -Mercaptoethanol(BME), 3-Mercaptopropionic acid (MPA), and 1-propanethiol(NPM). All these thiols (20mM) were added to the QD ( $0.2\mu\text{M}$ ) in aqueous phase so that the molar ratio of thiol/QD is  $10^5$ . The pH value of QD solution is 8.3. For transient absorption measurement and steady-state fluorescence measurement, the samples were placed in 3 mm quartz cell with absorbance about 0.3-0.4. However, for temperature dependent fluorescence measurement, the film samples were fabricated by conventional drop casting onto the glass substrates evaporated under vacuum ensuring the aging time short enough. The long aging time (24 hours incubation) sample is the same case.





**Figure 3-5. (a) The absorption and (b) the fluorescence spectra of CdSe/ZnS core/shell QDs used in this study. The B1 feature (first absorption peak) is around 550nm and the PL peak is around 565nm at room temperature.**



## Chapter 4 Results and discussion

### 4-1 Transient absorption

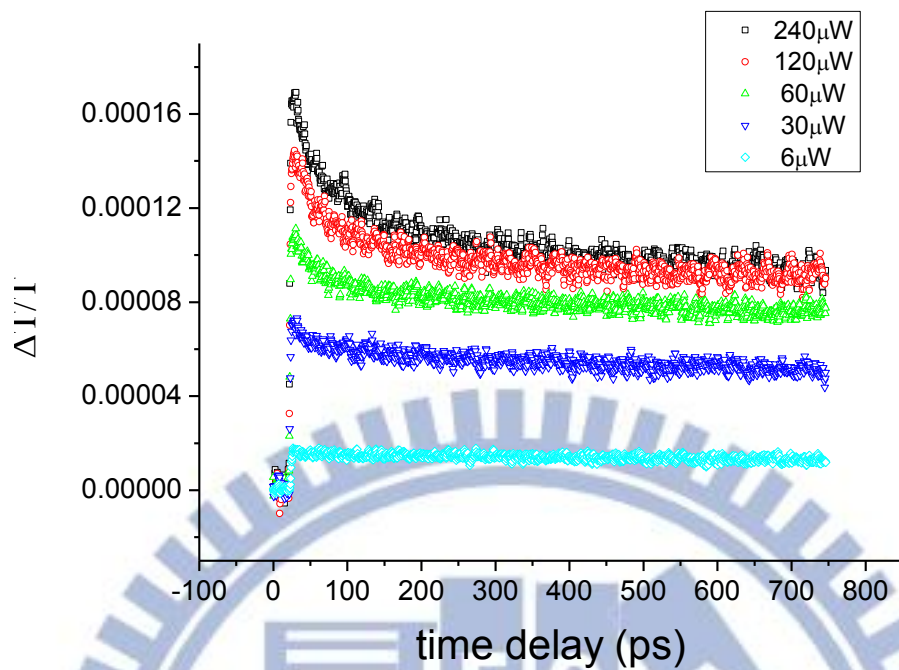
The transient absorption spectroscopy is a convenient tool for probing the charge recombination dynamics of semiconductor QDs. The absorption traces pumped at 400nm and probed at 565nm (first excitonic peak) are presented in Figure 4-1. Previous ultrafast studies of semiconductor QDs have shown that the transient absorption signals are strongest near the band edge [16]. The signal level in the measurements is  $\Delta I/I \sim 10^{-4}$ - $10^{-5}$  so that we can be readily detected. The bleaching recovery at the first excitonic peak has been employed to monitor the influence of surface modification as well as interfacial electron transfer processes. The time resolved absorption traces are fit by double exponential function: a fast one on the order of several tens of picoseconds, followed by a much longer one on the order of nanosecond. Mainly, the fast decay observed in the transient absorption signal was represented by variety of possible processes: electron-phonon coupling, charged carrier trapping or Auger recombination [42]. To confirm the photo-physics of this CdSe/ZnS core/shell QDs, we performed intensity dependent measurements [37]. If Auger recombination is a significant effect, we would expect that both the time constant and the relative amplitude of the fast decay depend on pump intensity [16, 42]. The higher pump power will correspond to shorter lifetime. Figure 4-1 shows transient absorption traces recorded at different pump intensities from QD in aqueous phase. The fast time constant does not depend on the pump intensity, for the range of power 0.03-0.24 $\mu$ J/pulse ( $\langle N_0 \rangle = 0.5$ -4). These results are not consistent with Auger recombination.

The above discussion implies that the fast decay for the CdSe/ZnS QDs arises from either trapping of charge carriers into defect states, presumable at the surface of

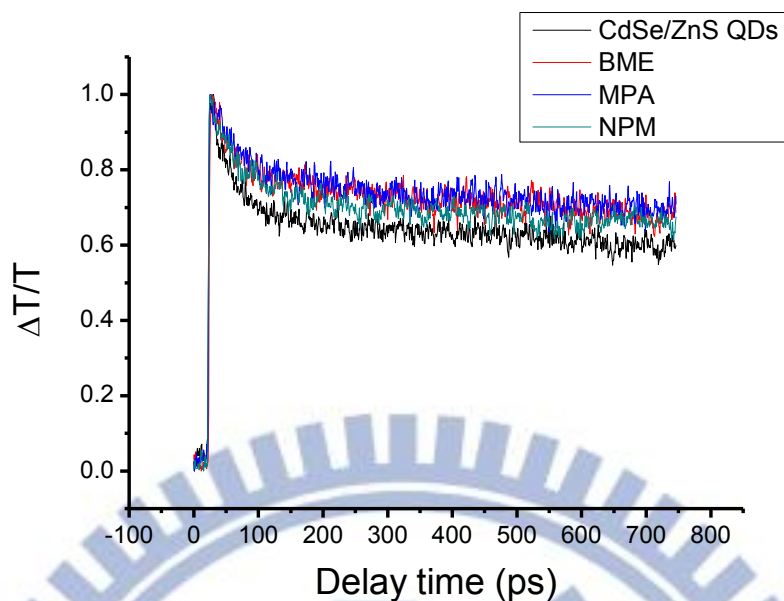
the QDs, or from electron-phonon coupling [2]. However, the electron-phonon coupling time constant for CdSe/ZnS QDs is usually in sub-ps. Thus, the electron-phonon coupling process should be complete within the time of the pump pulse in our experiments and cannot be responsible for this fast exponential decay. Therefore, the transient absorption trace in Figures 4-1 is assigned to charge carrier trapping at surface states in the CdSe/ZnS QDs. Figure 4-2 shows the enhancement in degree of surface passivation by thiols lead to slower dynamics of the single e-hole pair state, indicating that short-chain thiols affect the defect state at QD surface. Since the transient absorption trace take approximately 1hour to collect, we only perform the TA data of QD aged with thiols for 24hr. Double exponential function fitting result shown in table 4-1 for Figure 4-2. The average lifetime is calculated as

$$\tau = \frac{A_1\tau_1 + A_2\tau_2}{A_1 + A_2} \quad \text{Eq. (4-1)}$$

The average lifetime of original pure QDs is about 1.6 ns, lower than other thiol-containing QDs from 1.8 ns to 2.8 ns. It should be noted MPA show strongest surface passivation, where NPM only has little enhancement. In this experiment, we can only obtain electron dynamics ( $1P_e$  to  $1S_e$ ) yet nothing with hole dynamics.



**Figure 4-1.** Transient absorption traces at the  $1P_e$  to  $1S_e$  for the CdSe/ZnS QDs in aqueous phase taken with different pump laser powers (shown in the figure).



**Figure 4-2. Transient absorption spectra for CdSe/ZnS QDs with different short chain thiol-containing molecules at 24 hours aged.**

**Table 4-1. Show the double exponential function fitting parameters of Figure 4-2. The last row indicates the average decay lifetime.**

	H2O	BME	MPA	NPM
$A_1$	0.29169	0.26747	0.26603	0.31439
$\tau_1$ (ps)	36.96271	36.57142	37.22371	33.17446
$A_2$	0.64578	0.66737	0.63467	0.60236
$\tau_2$ (ps)	2307.994	3380.936	3964.77	2790.904
$\tau_{avg}$ (ps)	<b>1601.372</b>	<b>2424.069</b>	<b>2804.733</b>	<b>1845.169</b>

## 4-2 Steady-state fluorescence

The photoluminescence (PL) spectra were recorded by JASCO fluorescent FT-6300 at room temperature, operating at 400nm as the excitation source. Here we used 3 different molar ratio of thiol/QD  $\sim 10^5$ ,  $10^6$ , and  $10^7$ . The ratio  $10^5$  could cause blinking suppression of single QDs, while QDs direct quench the PL at ratio  $\sim 10^7$  observed in Jeong's experiment [11]. Since BME have been studied for a long time, this thiol was used in our thiol / QD molar concentration ratio experiment. Figure 4-3 shows the steady-state fluorescence spectra of three BME/QD concentration ratios vs. aging time.

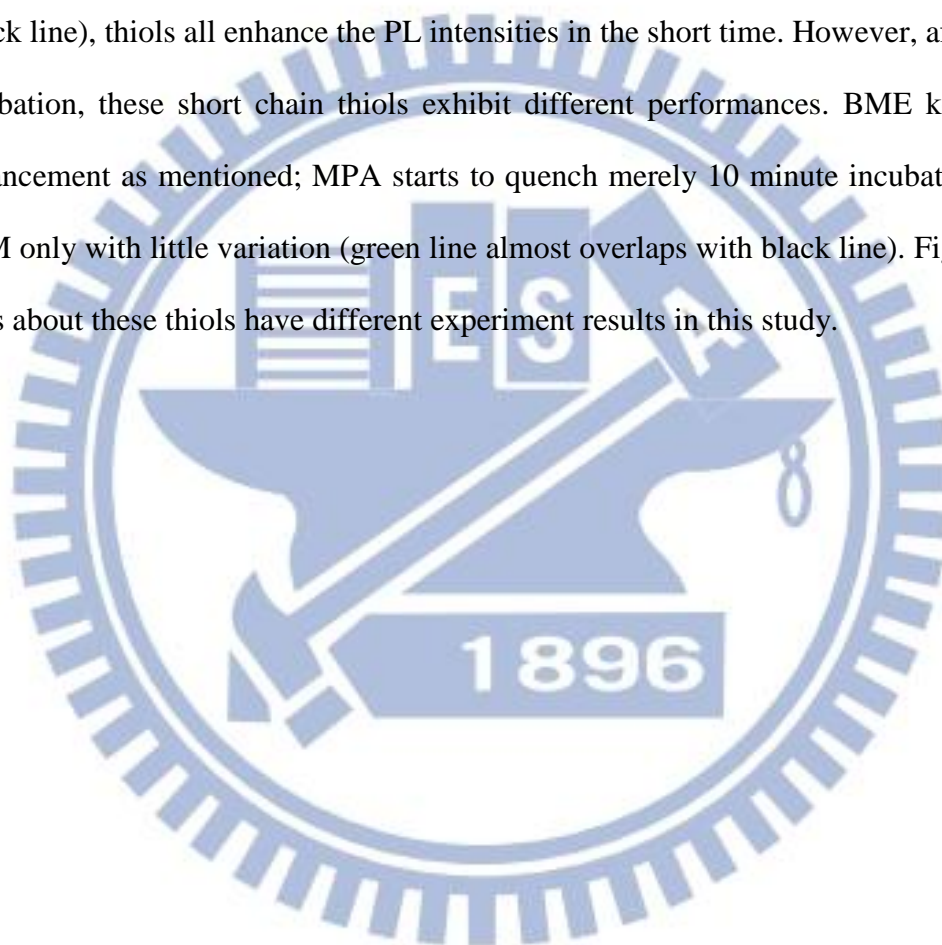
Obviously, comparing to pure QDs, other three lines show different trends. BME/QD concentration ratio  $\sim 10^5$  enhances PL vs. time while BME/QD ratio  $\sim 10^6$  enhances PL as soon as BME added, then quench PL slowly. However, the BME/QD ratio  $\sim 10^7$  quench directly. These three trends suggest the interaction of thiols capping on QDs surface.

The BME/QD  $10^5$  ratio shows PL enhancement, which could related to surface passivation via electrons donation to a surface trap state. Here, the BME interact with QD only by weaker coordination-type bonds through the sulfur lone-pair electrons. It would prevent the core electrons eject to the defect sites on the surface. At this ratio, BME will maintain thiol form, and keep blinking suppression thus PL keep the enhancement. At BME/QD ratio  $\sim 10^6$ , BME shows higher PL enhancement compare to  $10^5$ , but slowly quench which indicate a stronger covalent-type bonds was formed for long time incubation. Thiol form transfer to thiolate form and the new hole trap sites would be produced and PL decreased. At this BME/QD concentration ratio ( $10^6$ ), we could clearly see the competition of two mechanisms.

At highest BME concentration, BME is 7 order higher than QDs, BME thiol form transfer to thiolate immediately, and PL steady decreased. That means the thiolate

and QDs bound soon and loses the ability to suppress blinking. From these results, we could confirm the critical concentration of thiol/thiolate or coordination-type bonds /covalent-type bonds conversion and successfully combined to aging time.

Following we checked the differences of three thiol-containing molecules with QDs. Figure 4-4 shows the steady-state fluorescence spectra of three thiols with QDs vs. aging time. The thiol / QD molar concentration ratio is  $10^5$ . Compared to pure QDs (black line), thiols all enhance the PL intensities in the short time. However, after long incubation, these short chain thiols exhibit different performances. BME keeps PL enhancement as mentioned; MPA starts to quench merely 10 minute incubation; and NPM only with little variation (green line almost overlaps with black line). Figure 4-4 hints about these thiols have different experiment results in this study.



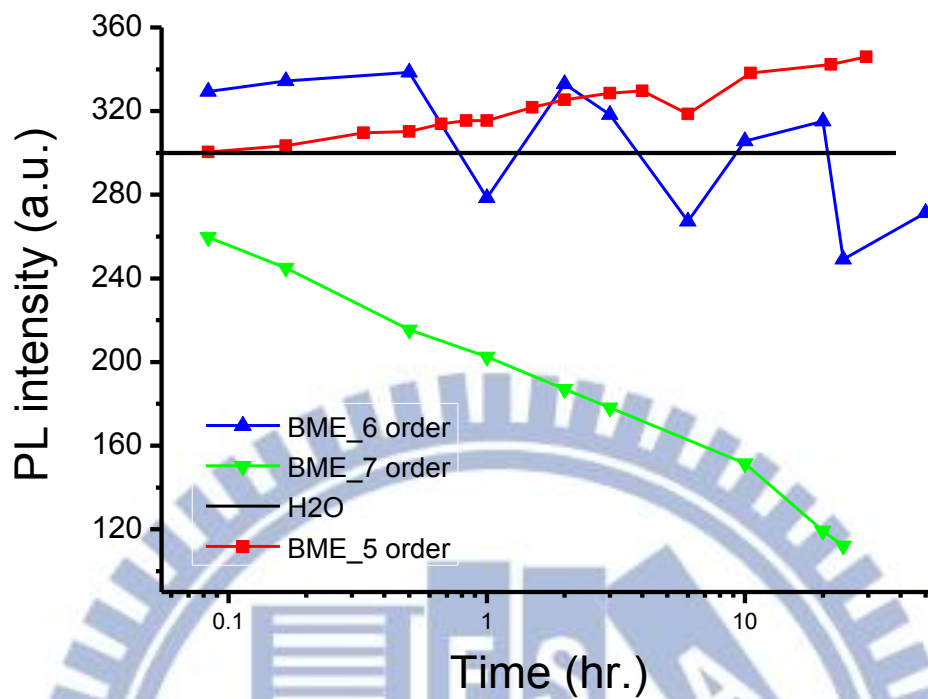


Figure 4-3. Steady-state fluorescence spectra of CdSe/ZnS QD with three different BME/QD molar concentration ratios vs. time.

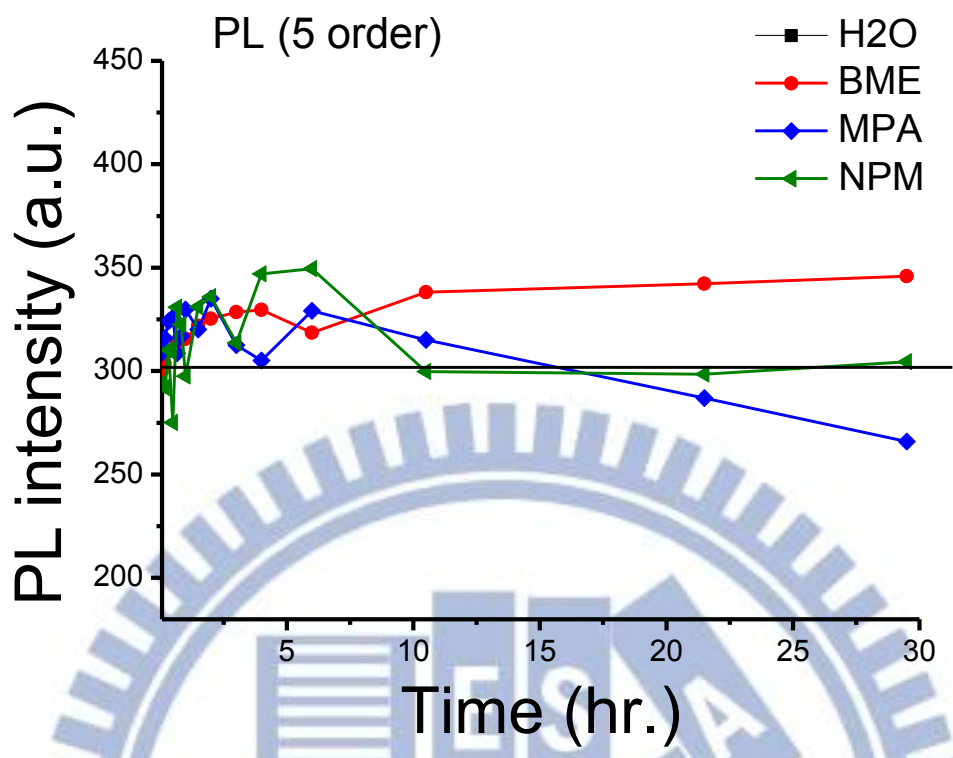


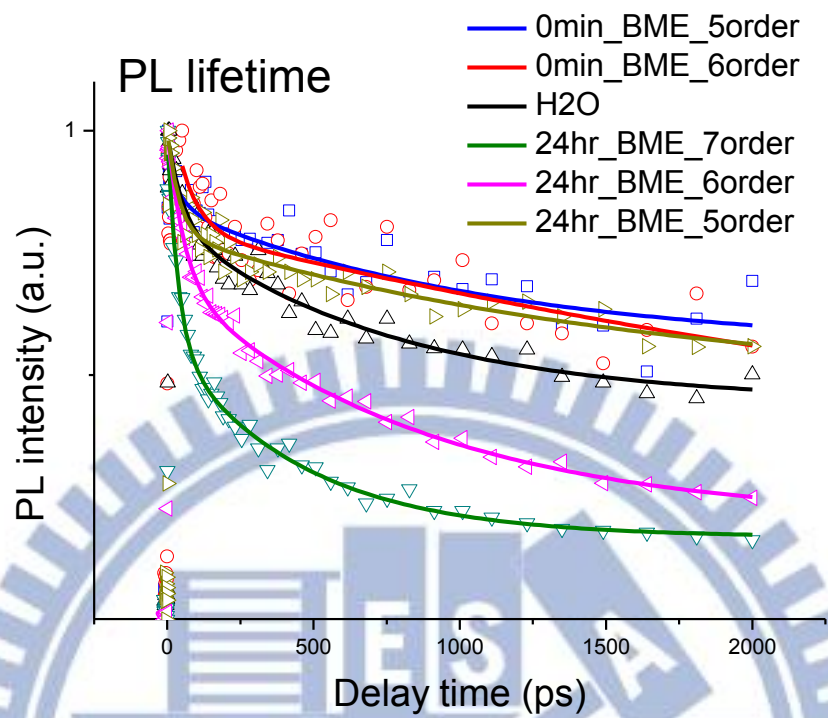
Figure 4-4. Steady-state fluorescence spectra of CdSe/ZnS QD with three short chain thiols (5 order concentration ratios) vs. time.



### 4-3 Time resolved photoluminescence

Transient absorption spectrum only used to study electrons dynamics. To monitor dynamics of photoexcited holes, the time-resolved photoluminescence (t-PL) measurement was used [11]. Here we used up-conversion technique to measure PL lifetime in several ns time scale. In the previous section, we studied three different BME/QD molar concentration ratios PL spectrum to confirm the relation of aging time and concentration. Now, the same condition (BME concentration and incubation time) was applied to further gain insight into the mechanism of PL increase/subsequent decrease/decrease directly. The experiment result was shown in Figure 4-5.

Compared to pure QDs (black line), 5 order and 6 order concentration BME have an increase in PL amplitude immediately. After 24 hours incubation, 6 order BME quenched and decay faster than pure QDs while 5 order BME only has little decrease, but its lifetime still longer than pure QDs. Finally we measured 7 order concentration of BME and obtained the shortest PL lifetime as expected. The amplitude enhancement/subsequent quench/quench directly of different concentration are well consistent with steady-state PL spectrum. An initial PL increase can be explained as a reduction in the number of electron traps and subsequent PL decline as formation of hole traps. The direct observation of electron trap passivation and its correlation with enhanced PL is unique in terms of connecting a specific thiol-QD interaction with a positive impact on QD PL.



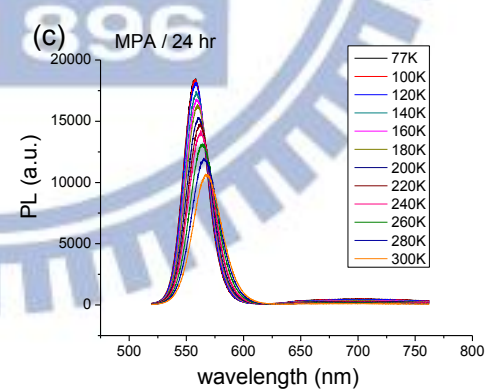
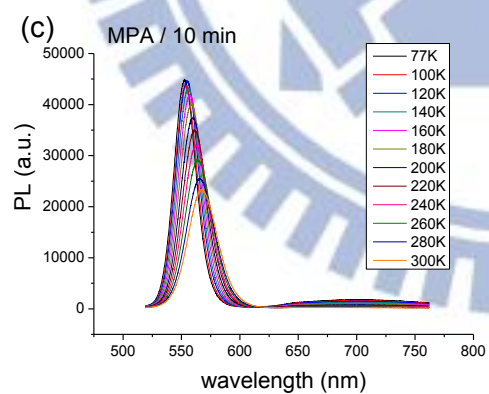
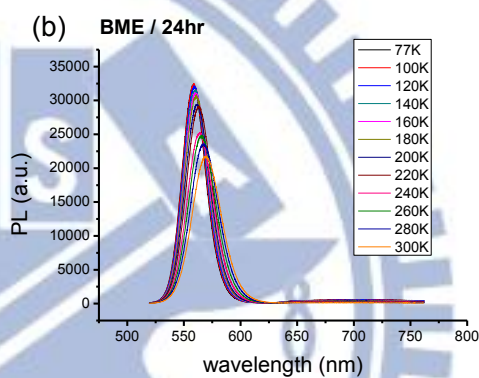
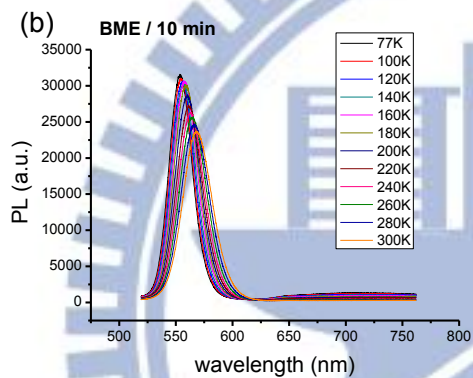
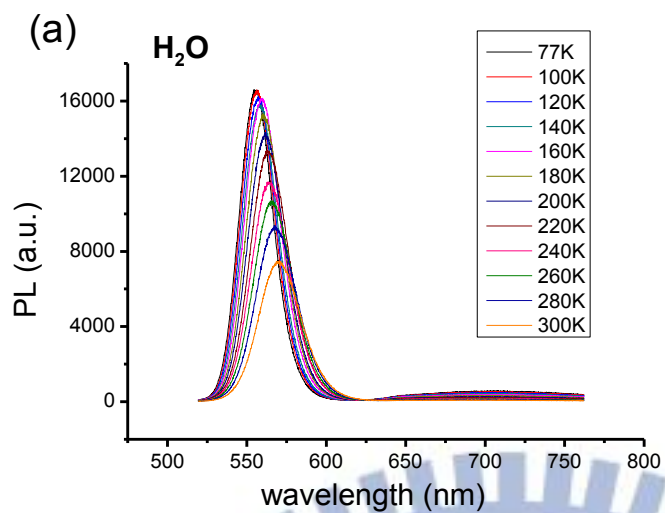
**Figure 4-5. Time-resolved photoluminescence spectra of CdSe/ZnS QD with three different BME/QD molar concentrations ratios and measured immediately and 24 hr incubation.**

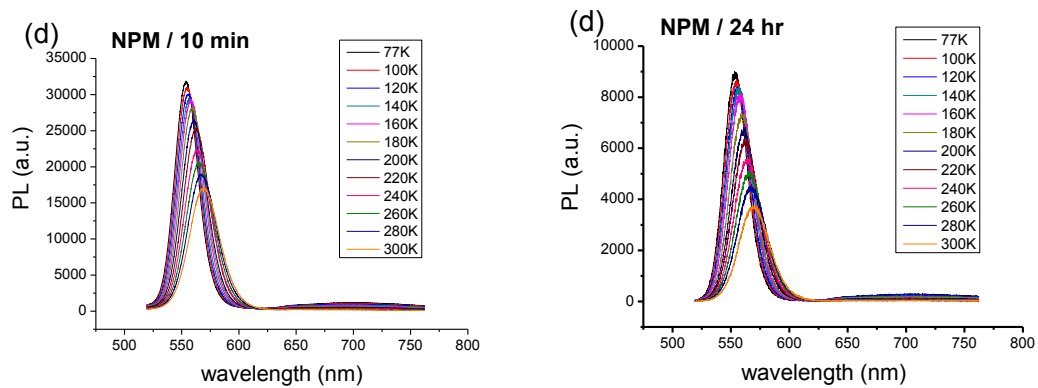
## 4-4 Temperature dependent fluorescence

### 4-4-1 Fluorescence intensity

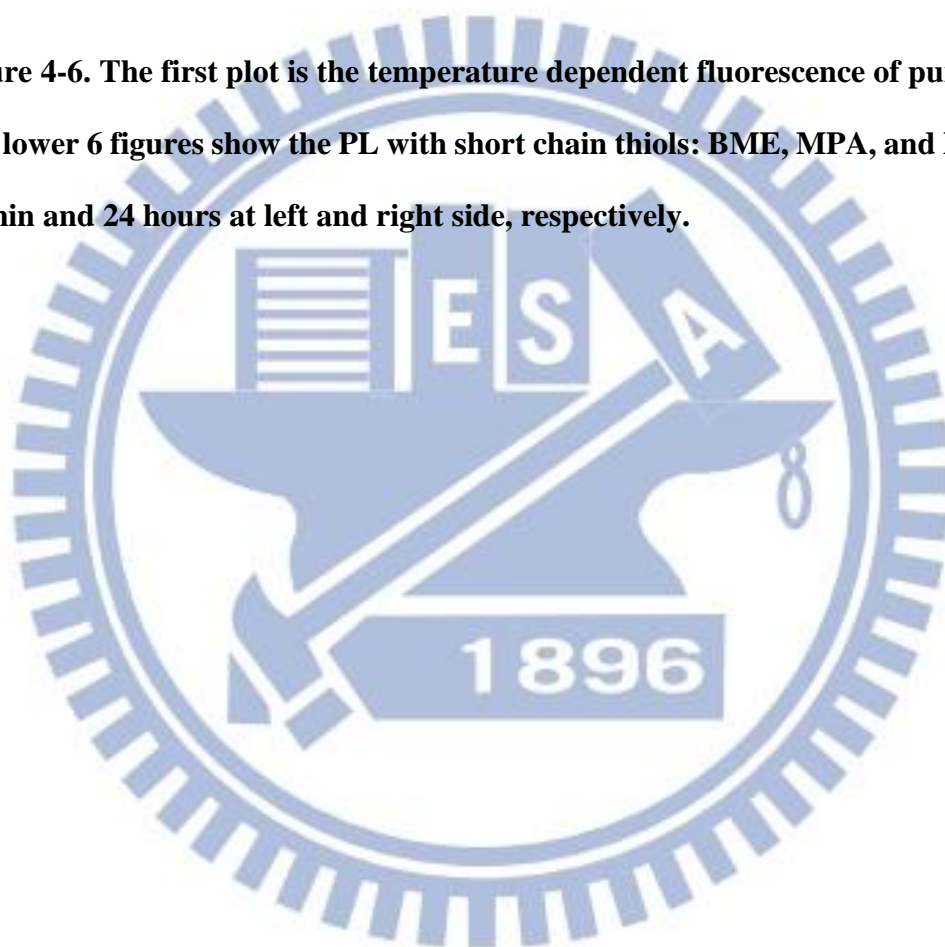
In the QDs and these thiols aging time line, we measure the temperature dependent PL at short time (10min) and long time (24hr). The temperature dependent fluorescence spectra of CdSe/ZnS and short chain thiol-capped QD film as a function of temperature from 77K to 300K, as shown in Figure 4-6. As the temperature increases, the PL spectra show a red-shift of the peak energy, increasing broadening and decreasing intensity. It is noteworthy that all the fluorescence properties are reversible in this temperature-dependent measurement.

These measurements, especially at low temperature, are important for revealing the influence of the thiol group on the PL properties, because PL measurements at low temperatures are sensitive to defects or localized states. Figure 4-6 (b), (c), and (d) shows the temperature dependence PL spectra of QDs with thiols. The defect-related PL band with a large Stokes shift of  $\sim 0.47$  eV is dominant at low temperatures, while the relative intensity of the band-edge PL increases with increasing temperature. There is no obvious change at defect-related PL band as soon as these thiols added (10min). However, 24hr later, the QDs defect intensity decrease with BME and MPA.





**Figure 4-6. The first plot is the temperature dependent fluorescence of pure QDs. The lower 6 figures show the PL with short chain thiols: BME, MPA, and NPM at 10 min and 24 hours at left and right side, respectively.**



Basically, some possible processes resulting in excited electron relaxations in the QDs including radiative relaxation, Auger nonradiative scattering, thermally activated trapping in surface and/ or defect/impurity states. In our experiments, the excitation density was very low and thus Auger scattering could be ruled out. Therefore, the nonradiative relaxation is most likely due to thermal activation of nonradiative trapping, which are often observed in semiconductor bulk, quantum dots and core/shell structure quantum dots [43].

At low temperatures, the non-radiative channel is not thermally activated so that the excited electrons can radiatively relax and emit photons. Once the temperature is increased, the nonradiative channels are thermally activated, such as trapping by surface/defect/ionized impurity states, as expressed below:

$$\tau_{NR} = \tau_0 \exp\left(\frac{E_a}{K_B T}\right) \quad \text{Eq. (4-2)}$$

Where  $E_a$  is the activation energy and  $K_B$  is Boltzmann's constant. The quantum efficiency can be expressed as:

$$\eta = \left(1 + \frac{\tau_R}{\tau_{NR}}\right)^{-1} \quad \text{Eq. (4-3)}$$

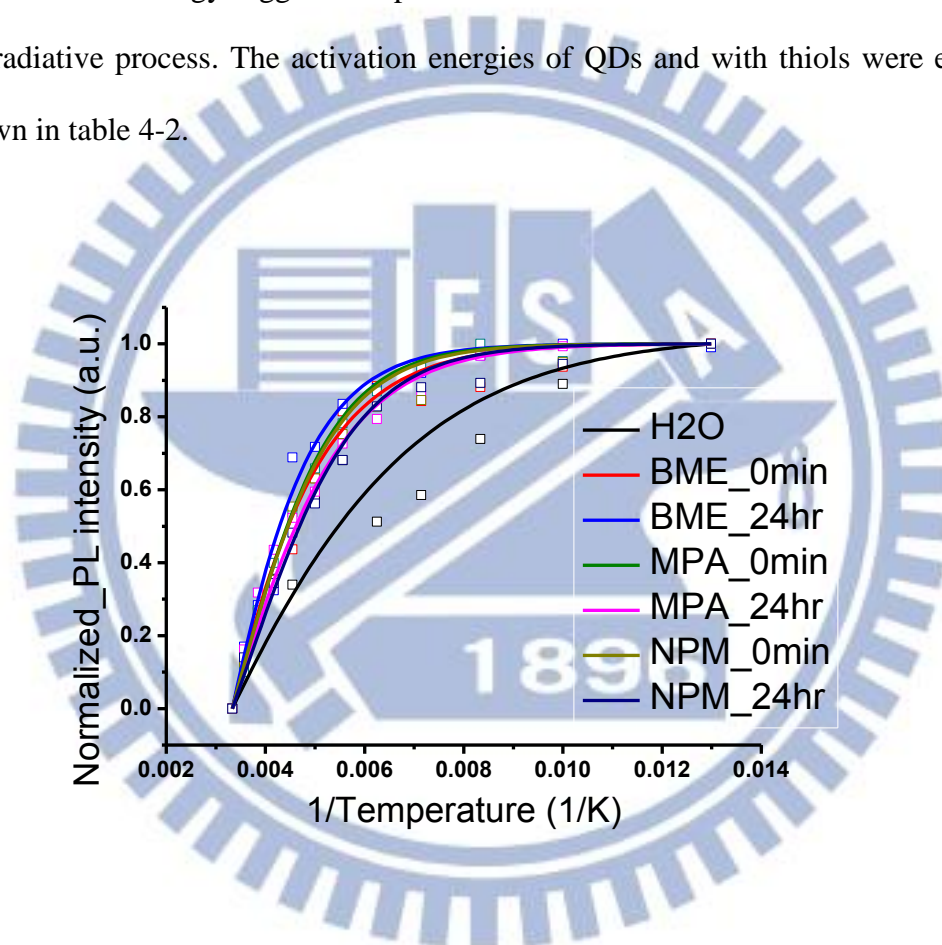
Where  $\tau_R$  and  $\tau_{NR}$  are radiative and nonradiative lifetimes, respectively. From equation 4-2 and 4-3, the nonradiative lifetime decreases with and increasing temperature, which result in a decreasing in the quantum efficiency and fluorescence intensity.

To further study the fluorescence spectra, a single Gaussian function was used to fit the band-edge PL peak. Figure 4-7 is the Arrhenius plot of the QDs with thiols fluorescence intensity from Gaussian function fitting. These fluorescence intensity

(arbitrary unit) vs. reciprocal temperature points (1/K) were fit using equation shown below,

$$I = I_0 \frac{1}{1 + \frac{\tau_R}{\tau_0} \exp\left(-\frac{E_a}{K_B T}\right)} \quad \text{Eq. (4-4)}$$

The activation energy suggests the probable barrier of excited electron relaxes through nonradiative process. The activation energies of QDs and with thiols were extracted shown in table 4-2.



**Figure 4-7. Arrhenius plot of fluorescence intensity for the edge-band of QDs with thiols. Evidently, pure QDs (black line) and BME, MPA, and NPM with 10 min and 24 hours (color line) incubation have large variation.**

**Table 4-2. Shows the activation energy of QDs and with thiols extracted from fluorescence intensity fitting curve in figure 4-7.**

	Pure QD	BME_10min	BME_24hr	MPA_10min	MPA_24hr	NPM_10min	NPM_24hr
$E_a$	35.597	64.953	82.404	83.489	65.385	79.399	74.441
(meV)	(±6.9364)	(±7.1277)	(±9.3121)	(±3.1248)	(±5.6764)	(±5.5777)	(±4.6120)

According to table 4-2, the activation energy of pure QDs is 35meV, which is smaller than normal semiconductor quantum dots without shell and polymer surrounded [44, 45]. It indicates that decreasing surface defect due to protection and stabilization cause high fluorescence quantum efficiency at room temperature [10]. It was also found the thiols change the surface electronic state of QDs as soon as the thiols added. This result shows that the short-chain thiols contact to the QDs will change the surface state of QDs immediately. That has the same phenomenon compared to QDs blinking suppression of BME [12]. However, it seems to no rule at different thiols aging time. As we know, thiols with electric cloud reduced defect trap site immediately and thiolate provided new defects after long aging time. The surface distribution of QD is changing so we couldn't find the rule of activation energy vs. time. All the activation energies of QDs with thiol-molecules increased, hinted QDs with thiols get harder to lose energies through nonradiative decay.



#### 4-4-2 Energy gap variation

In semiconductor nanostructures, the temperature dependence of the energy gap is usually similar to the bulk semiconductor type, except for a temperature-independent energy off-set due to the quantum confinement [41]. Usually, the temperature dependence of peak energy in quantum dots, nanorods and core/shell quantum dots can be expressed by the empirical Varshni relation [46]:

$$E_g(T) = E_g(0) - \frac{\alpha T^2}{T + \beta} \quad \text{Eq. (4-5)}$$

Where  $E_g(0)$  is the band gap at zero temperatures,  $\alpha$  is the temperature coefficient, and  $\beta$  is a parameter related to the Debye temperature.

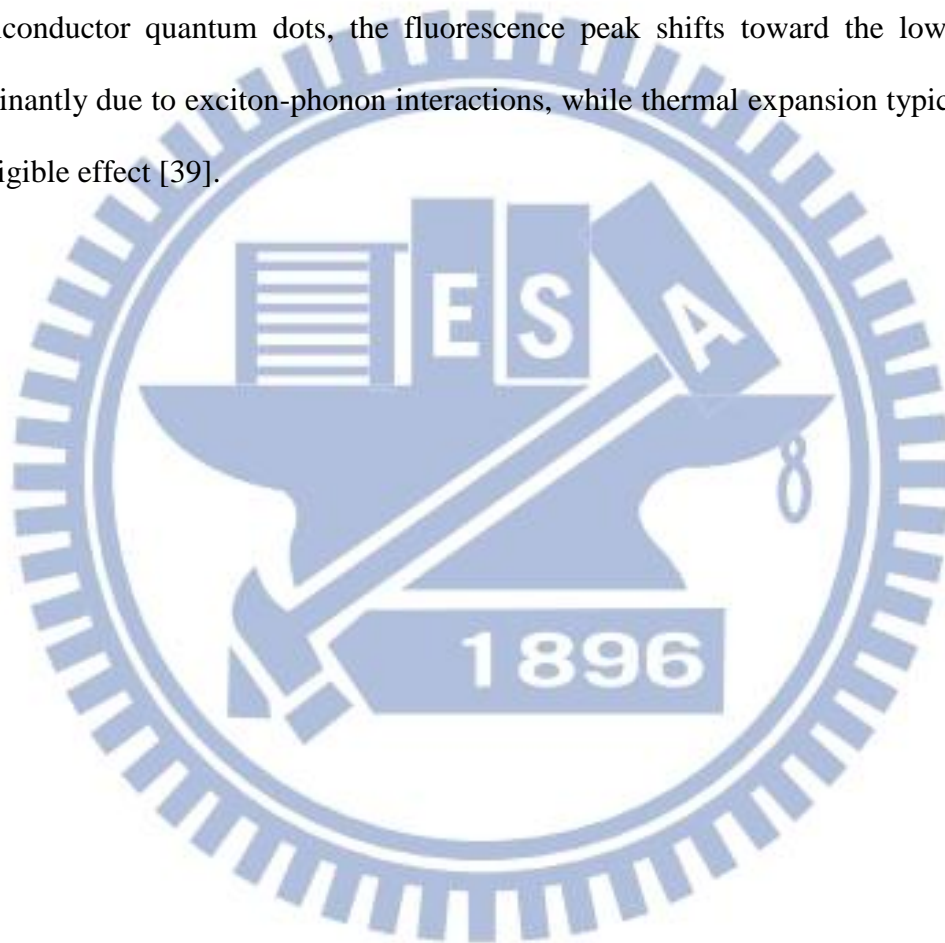
An improved expression proposed by O'Donnell and Chen is also used for described temperature dependence of the band gap in core/shell quantum dots [47], which is based on the analysis of the electron-phonon coupling mechanism responsible for the band gap shift:

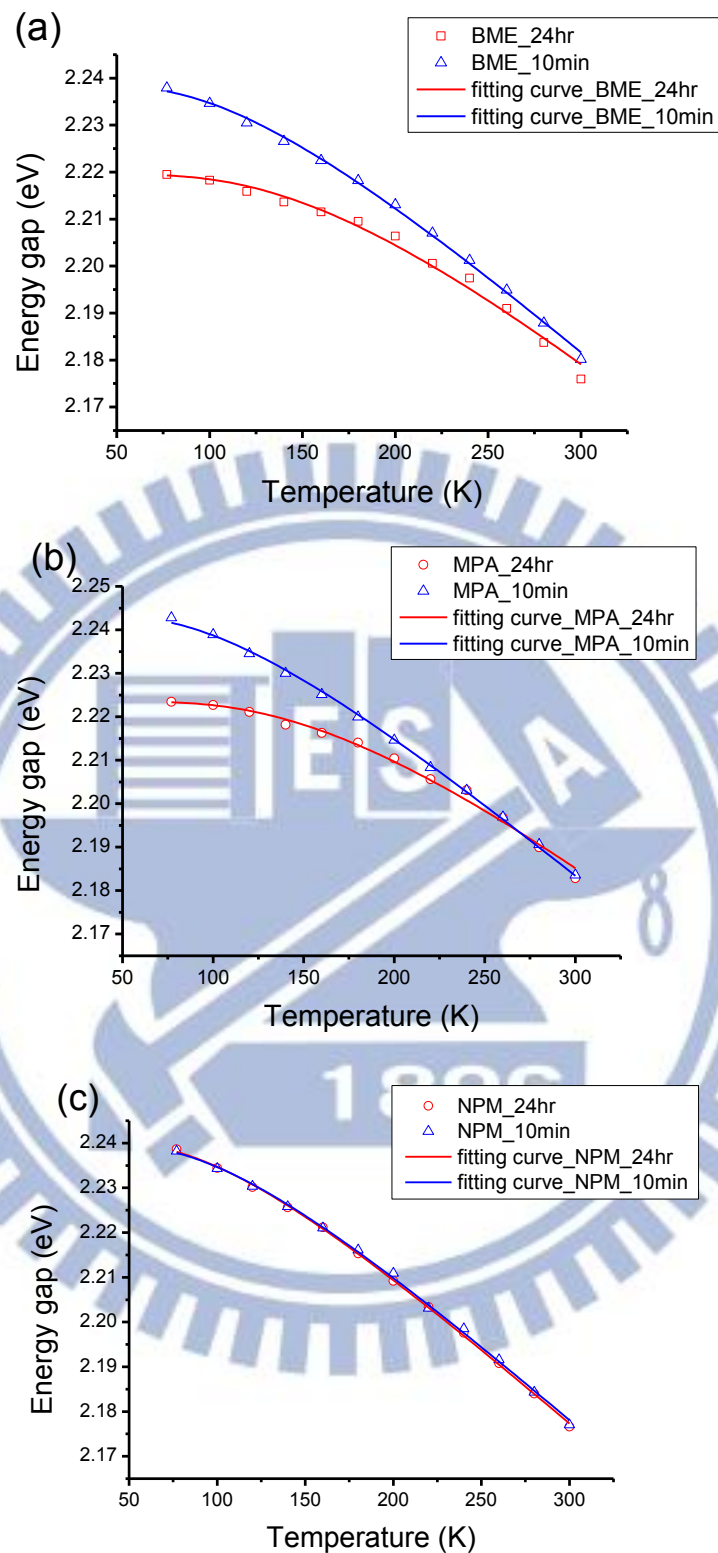
$$E_g(T) = E_g(0) - \frac{2S \langle \hbar\omega \rangle}{\exp\left(\frac{\hbar\omega}{k_B T}\right) - 1} \quad \text{Eq. (4-6)}$$

Where  $S$  is the Huang-Rhys factor that represents the strength of exciton-phonon coupling. The higher the Huang-Rhys factor, the stronger the coupling.  $\langle \hbar\omega \rangle$  is the average phonon energy. According to the theoretical analysis carried out by Schmitt-Rink and co-workers [48], the coupling is proportional to  $\alpha_0^3/V$ , where  $\alpha_0$  is the Bohr radius and  $V$  is the volume of the nanocrystal, leading to an increase in the value of  $S$  as the size of the nanocrystal is decreased.

We also extracted the energy gap (eV) vs. temperature (K) from single Gaussian

fitting of temperature dependent fluorescence. The fluorescence peak energy of QDs and thiols added as a function of temperature with fitting line (equation 4-6) is shown in Figure 4-8. It was found that the peak energy of fluorescence exhibits a red shift  $\sim 57\text{meV}$  with increasing temperature from 77K to room temperature. Two mechanisms that are responsible for the temperature-dependent energy gaps are renormalization of band energies by electron-phonon interactions and thermal lattice expansion. In semiconductor quantum dots, the fluorescence peak shifts toward the low energy dominantly due to exciton-phonon interactions, while thermal expansion typically has negligible effect [39].





**Figure 3-8. The energy gap extracted from PL curve fitted with single Gaussian as a function of temperature. All thiols: (a) BME (b) MPA (NPM) measured for immediately and 24 hr. incubation**

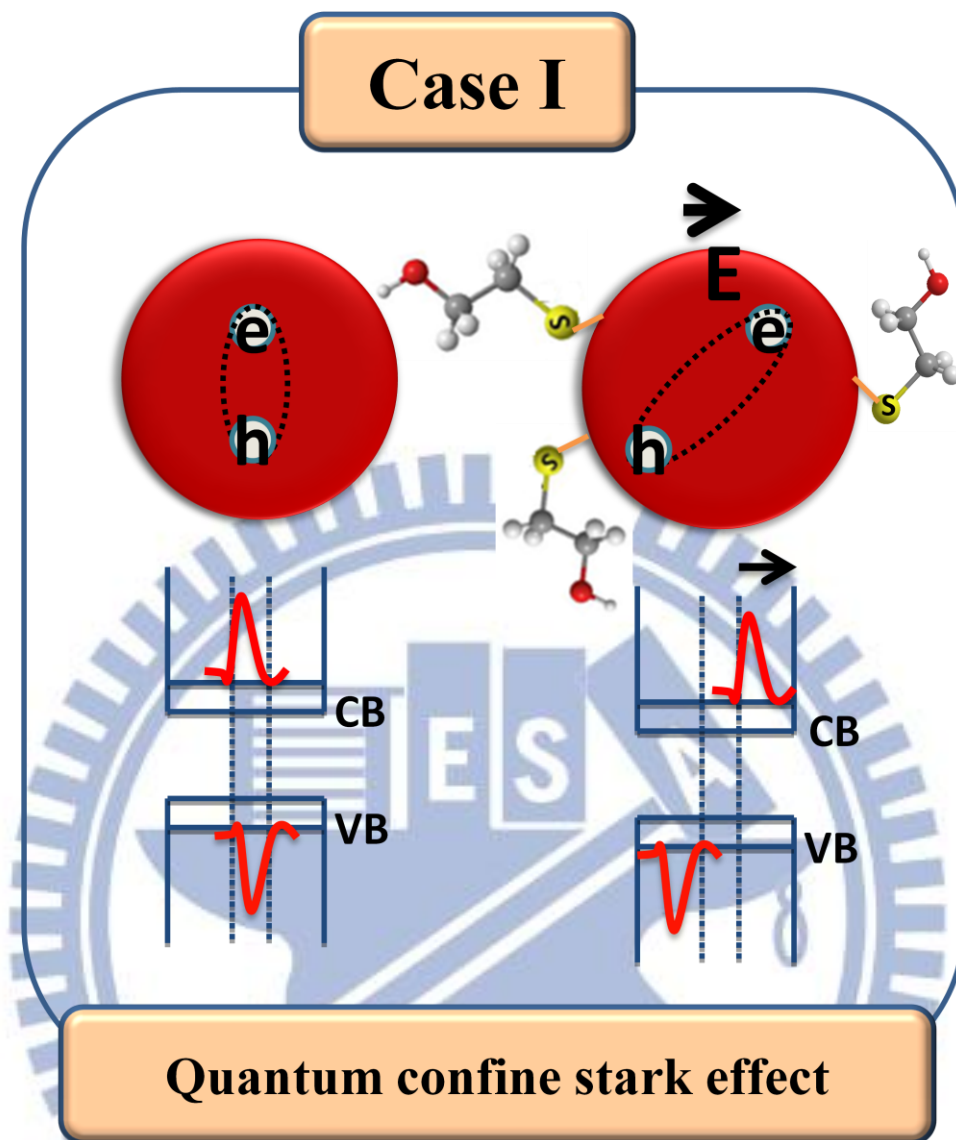
Parameters used in the fit of the photoluminescence peak energy as a function of temperature by equation 4-6 were summarized in table 4-3. Obviously, after long aging time with thiol molecules, it was found that the bandgap at zero temperature  $E_g(0)$  exhibits a little red shift. BME shift  $\sim 20$  meV and MPA shift  $\sim 22$  meV, while NPM shows no difference. It was suggested that two possible reasons might be used to explain the red shift phenomenon after thiols long aged. The first is dependent on the dipole created by inhomogeneous capping ligand exchange of QDs surface [5, 6, 49]. The inhomogeneous surface distribution will produced ligand-induced internal electric fields or the quantum-confined stark effect (QCSE). We consider that internal electric field pull/push electron and hole wave functions to different parts within the QDs volume, and hence the energy levels are changed, leading to a red shift of the optical band gap illustrated in Figure 4-9 (a). It could be viewed as first exciton binding energy decreases.

Another reason was attribute to hole transferred and trapped on the surface as covalent-type bonds was formed for thiols long time incubation. The same, electron-hole pair would be separated then reduced the wave function overlap. The first exciton binding energy reduced as before shown in Figure 4-9 (b).

Besides, the Huang–Rhys factor  $S$  and the average phonon energy  $\langle \hbar\omega \rangle$  of BME- and MPA-capped QDs with aged time 24 hours show larger than that of pure QDs, which means they had higher exciton-phonon coupling, while the NPM-capped QD without any changes. These two factors indicate acoustic phonon and optical phonon average behavior [4].

**Table 1-3. Fit parameters of the energy gap variation in QDs temperature dependent fluorescence measurement. It was fit using equation 4-6.**

	<b>Pure QD</b>	<b>BME 10min</b>	<b>BME 24hr</b>	<b>MPA 10min</b>	<b>MPA 24hr</b>	<b>NPM 10min</b>	<b>NPM 24hr</b>
$E_g(0)$ (eV)	2.231 ( $\pm 0.0013$ )	2.238 ( $\pm 0.0008$ )	2.218 ( $\pm 0.0007$ )	2.245 ( $\pm 0.0005$ )	2.223 ( $\pm 0.0007$ )	2.239 ( $\pm 0.0008$ )	2.240 ( $\pm 0.0006$ )
<b>S</b>	2.095 ( $\pm 0.1377$ )	2.183 ( $\pm 0.1011$ )	3.035 ( $\pm 0.3855$ )	1.940 ( $\pm 0.0364$ )	2.651 ( $\pm 0.3043$ )	2.175 ( $\pm 0.0757$ )	2.112 ( $\pm 0.0489$ )
$\langle \hbar\omega \rangle$ (meV)	30.936 ( $\pm 3.2304$ )	32.311 ( $\pm 2.2252$ )	58.889 ( $\pm 4.7976$ )	24.107 ( $\pm 1.0679$ )	55.892 ( $\pm 4.4085$ )	28.646 ( $\pm 1.7841$ )	26.313 ( $\pm 1.2460$ )



**Figure 4-9(a).** Scheme of ligand induced internal electric fields or QCSE separates the electron and hole wave functions and therefore decreases the first exciton energy (red shift).

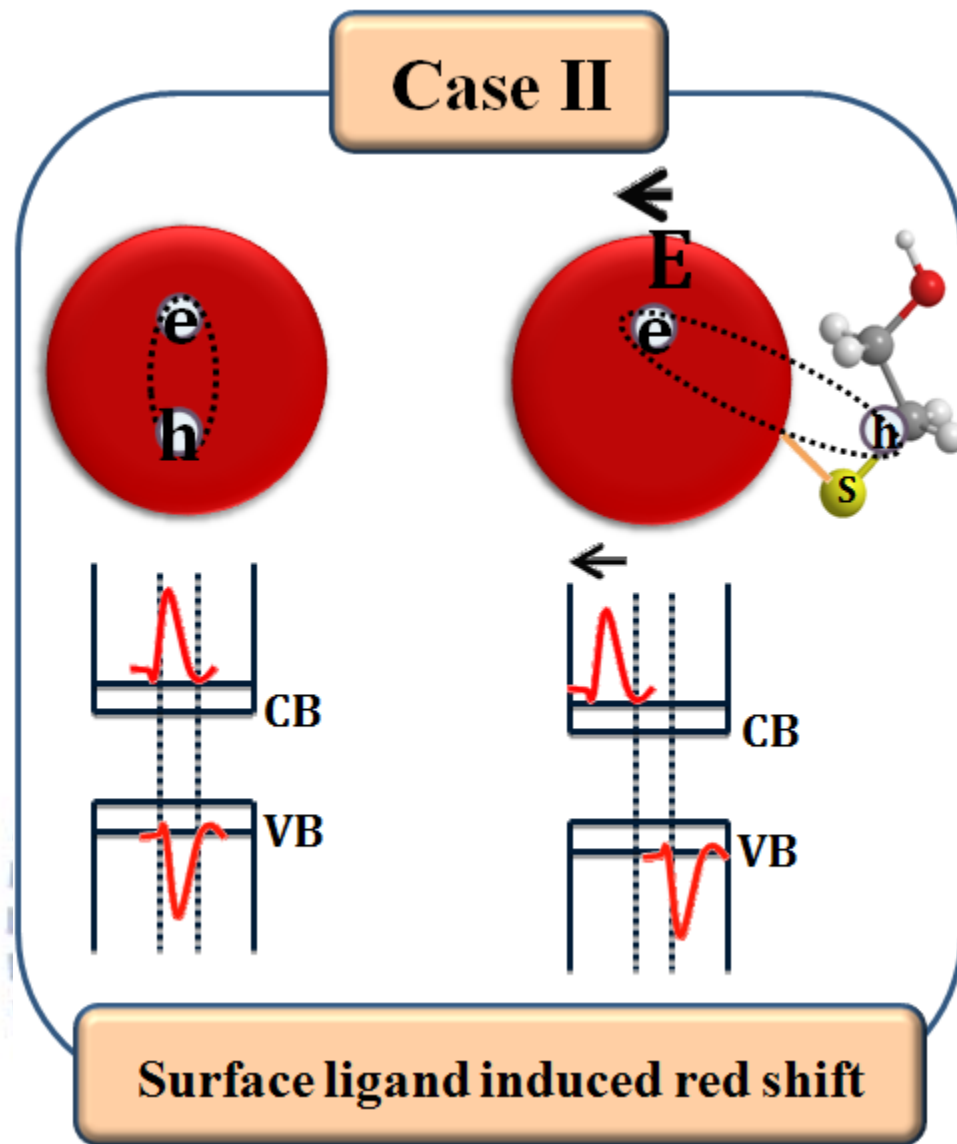


Figure 4-9(b). Scheme of surface ligand induced hole transferred and trapped on the surface as covalent-type bonds was formed. Therefore, electron and hole separate and the energy gap red shift as case one.

#### 4-4-3 Band width of fluorescence

The band width of fluorescence was also investigated as a function of temperatures. Figure 4-10 show the full width at half-maximum (FWHM) increases with increasing temperature, around 18meV from 77K to 300K. Previous studies on the temperature dependence of the emission FWHM in semiconductor quantum dots and nanocrystals have shown that the broadening of the broadening of the emission peak can be separated into inhomogeneous and homogeneous parts.

Inhomogeneous broadening originates from the fluctuations in size, shape and composition of the quantum dots and is temperature independent. Homogeneous broadening, on the other hand, is temperature dependent, and is related to exciton scattering by acoustic and optical phonons. Exciton–phonon interactions and ionized impurity scattering can result in bandwidth broadening in semiconductor nanoparticles that should be temperature dependent has been extensively investigated [38]. The overall broadening is described as

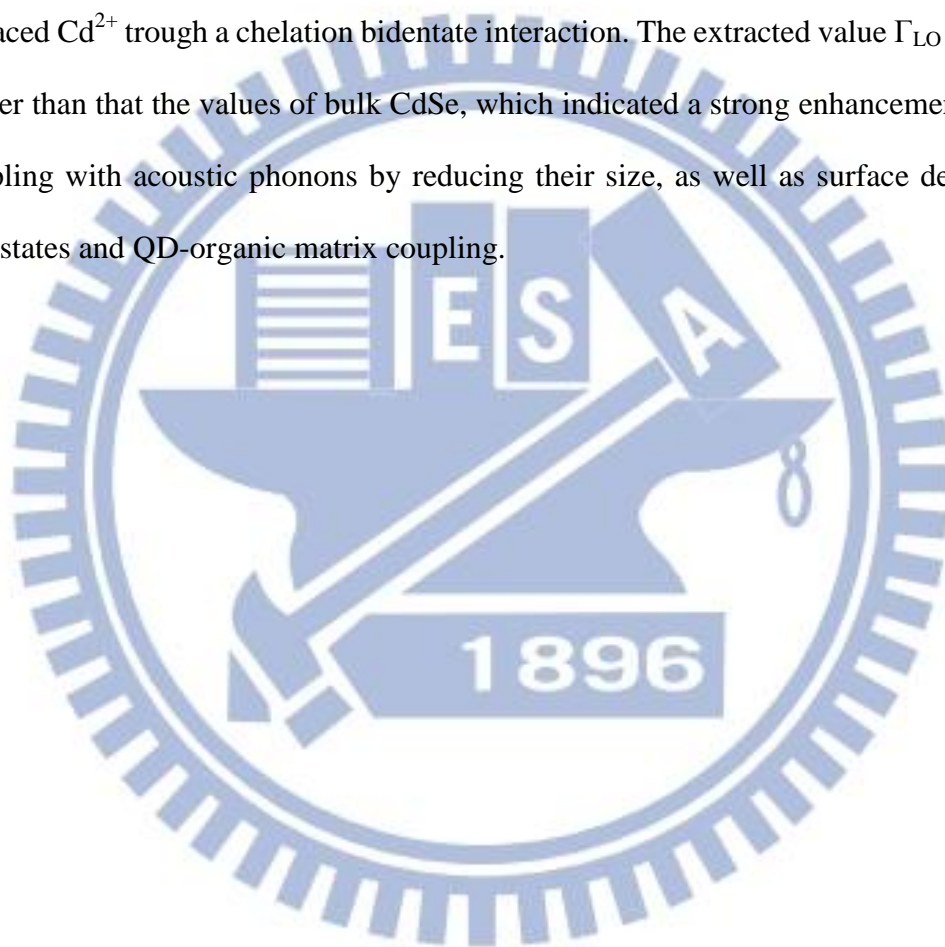
$$\Gamma(0) = \Gamma_{inh} + \sigma T + \frac{\Gamma_{LO}}{(\exp(\frac{E_{LO}}{k_B T}) - 1)^m} \quad \text{Eq. (4-7)}$$

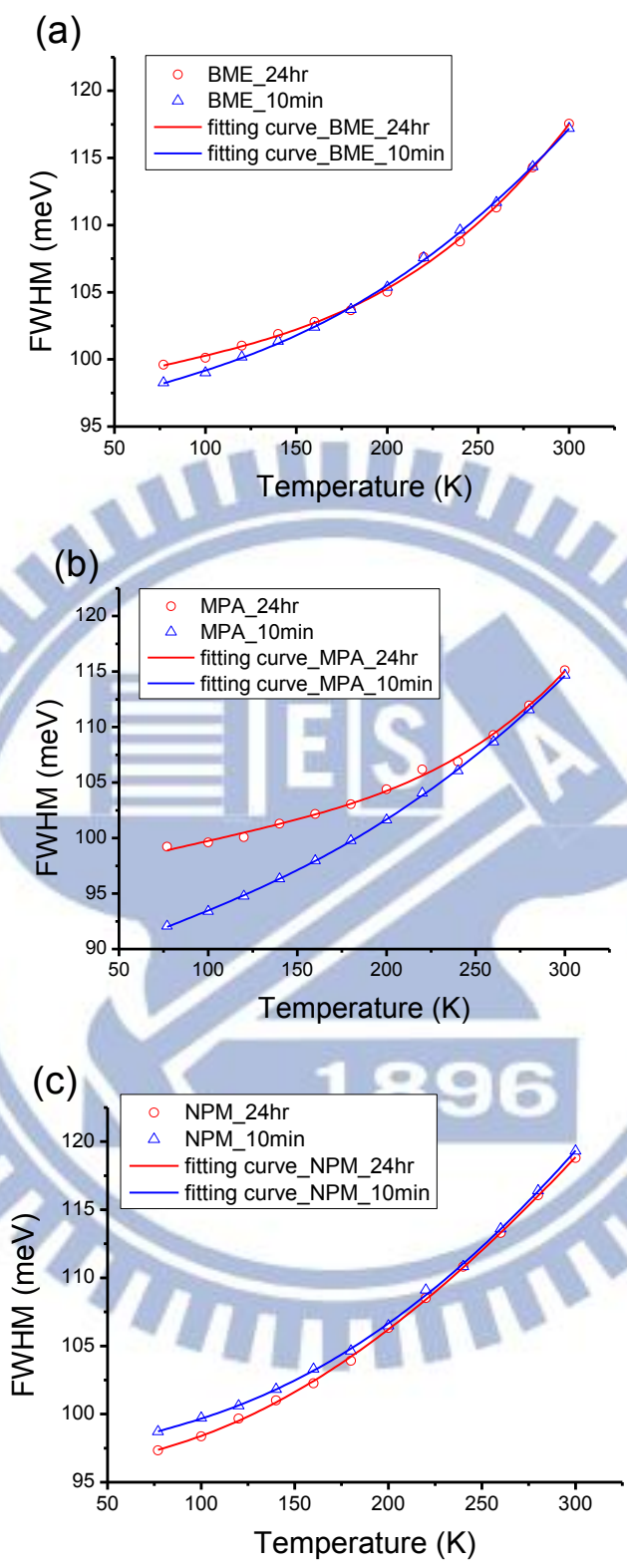
where  $\Gamma_{inh}$  is the inhomogeneous broadening and the last two terms represent homogeneous broadening due to acoustic and optical phonon scattering;  $\sigma$  is the excitonic–acoustic phonon coupling coefficient,  $m$  is the number of LO phonons involved in thermal escape of carriers ;  $\Gamma_{LO}$  represents the strength of exciton–LO phonon coupling and  $E_{LO}$  is the LO phonon energy. Due to the different dependence of the terms on temperature, acoustic phonons play a dominant role at low temperatures, while the optical phonons contribute at the higher temperatures.

The FWHM fitting parameters of Figure 4-10 were summarized in table 4-4. It



is interesting that the  $\Gamma_{inh}$  become smaller measured at addition of thiols immediately followed become large after 24hours incubation for BME-and MPA-capped QDs. The initial  $\Gamma_{inh}$  reduced could be attributed to surface passivation of the QDs via coordination-type bonds through the sulfur lone-pair electrons. For long time incubation, the stronger covalent-type bonds was formed and the new hole traps would be produced to cause the  $\Gamma_{inh}$  increase again. Here, the carboxylate group bound to a surfaced  $Cd^{2+}$  trough a chelation bidentate interaction. The extracted value  $\Gamma_{LO}$  is much higher than that the values of bulk CdSe, which indicated a strong enhancement of the coupling with acoustic phonons by reducing their size, as well as surface defects or trap states and QD-organic matrix coupling.





**Figure 4-10. FWHM bandwidth (dots) as a function of temperature and fit by equation 4-7 (solid lines) of QDs with (a) BME-capped (b) MPA-capped (c) NPM-capped.**

**Table 4-4. Parameters used in the fit of the photoluminescence FWHM as a function of temperature by equation 4-7**

	Pure QD	BME_ 10min	BME_ 24hr	MPA_ 10min	MPA_ 24hr	NPM_ 10min	NPM_ 24hr
$\Gamma_{inh}$ (meV)	98.544 ( $\pm 1.0796$ )	95.289 ( $\pm 0.5200$ )	97.060 ( $\pm 0.7313$ )	87.188 ( $\pm 0.3591$ )	96.143 ( $\pm 0.6495$ )	96.137 ( $\pm 0.7641$ )	94.941 ( $\pm 0.9207$ )
$\alpha$ ( $\mu\text{eV}/\text{K}$ )	44.600 ( $\pm 10.443$ )	37.795 ( $\pm 5.5248$ )	30.690 ( $\pm 6.9135$ )	62.296 ( $\pm 3.6928$ )	36.490 ( $\pm 5.4949$ )	33.188 ( $\pm 8.6180$ )	30.190 ( $\pm 11.427$ )
$\Gamma_{LO}$ (meV)	26.000 ( $\pm 3.3766$ )	26.988 ( $\pm 1.1013$ )	36.368 ( $\pm 2.7762$ )	23.760 ( $\pm 0.7830$ )	36.761 ( $\pm 6.7437$ )	29.973 ( $\pm 1.8716$ )	30.324 ( $\pm 3.0378$ )

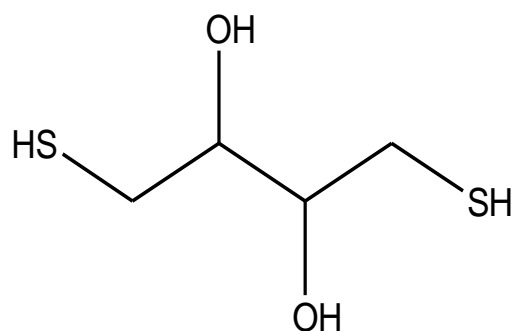


## Chapter 5 Recommendation for Further Work and

### Summary

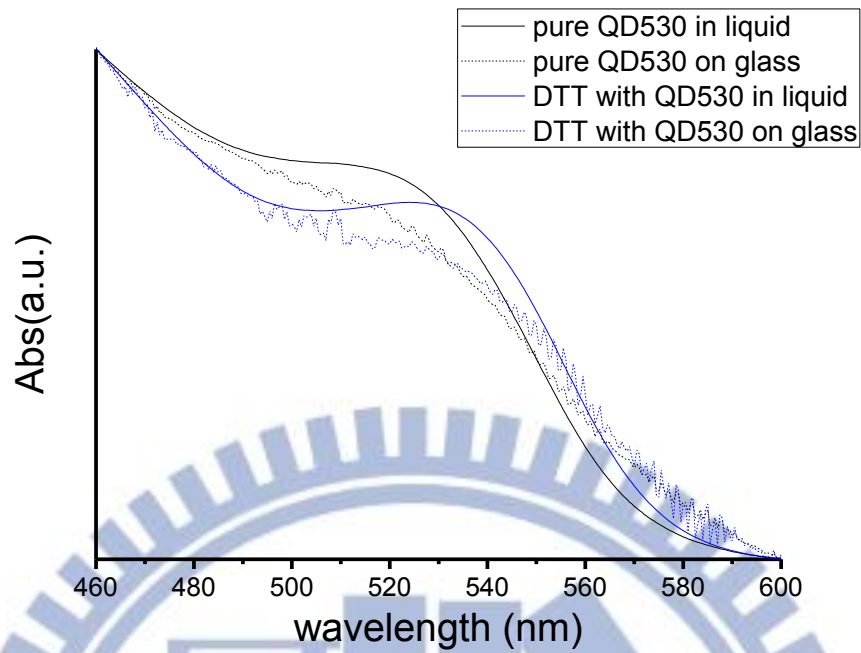
#### 5-1 Electronic coupling in CdSe/CdS film

Though the samples under investigation are aqueous solution, we must consider the highly applications of samples in solid state. Films of colloidal quantum dots (QDs), often called QD solids, have recently experienced a significant increase in attention for the devices applications. Normally, the QDs are electronically coupled by removing or replacing the original bulky surfactants to decrease the inter-particle distances result in overlapping wave functions and increasing the mobility of charge carriers. In the final part of experiments, we studied the absorbance spectrum and transient absorption pump-probe spectrum of the Dithiothreitol (DTT) with CdSe/CdS core/shell QDs film. This dithiol molecule was used to further study the functions of thiol group. Figure 5-1 shows the formula of DTT. The CdSe/CdS core shell QDs were surrounded by citrate and replaced by DTT. After four sizes of CdSe QDs with DTT were drop-casting on glass, we studied the room temperature absorbance. The films composed of QDs with first exciton transitions at 2.19eV, 2.28eV, 2.35eV and 2.36eV, corresponding to QD radii of 3.5nm, 3.1nm, 2.8nm, and 2.8nm, respectively.



**Figure 5-1. Showing the formula of dithiothreitol (DTT).**

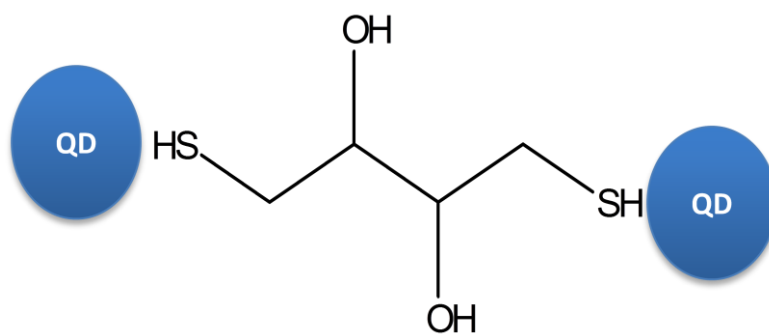
Figure 5-2 shows the room temperature absorbance of the 2.35eV QD film. Obviously, the DTT treatment causes the lowest energy transition to red shift by ~380meV compared to untreated film. A red shift can arise from exciton delocalization, dipole-dipole interactions, which would lower the transition energy, or difference in dielectric screening in the films compared to solution [50]. Besides, the spectrum of the QD solids shows significant broadening with respect to the spectrum of the dispersion, but clearly still exhibits quantum confinement. Such a broadening could be due to increased polydispersity, disorder in dielectric environment resulting in a spatial variation of polarization energies or strong electronic coupling [51]. The first exciton transition peak was fitted by single Gaussian function. Table 5-1 displays the peak position and band width of pure QDs and DTT treated film in 4 different sizes. The high peak variation (red shift up to 500meV) suggested the strongly electronic coupling. A possible reason is that DTT with two thiol group at the ends of chain thus a DTT connected to two QD particles, enhanced QDs coupling. The schematic diagram shows in Figure 5-3.



**Figure 5-2. Absorbance of liquid (solid line) and solid (dotted line) for CdSe/CdS QDs ( $E_g = 2.35\text{eV}$ ) in citrate (black) and in DTT (blue).**

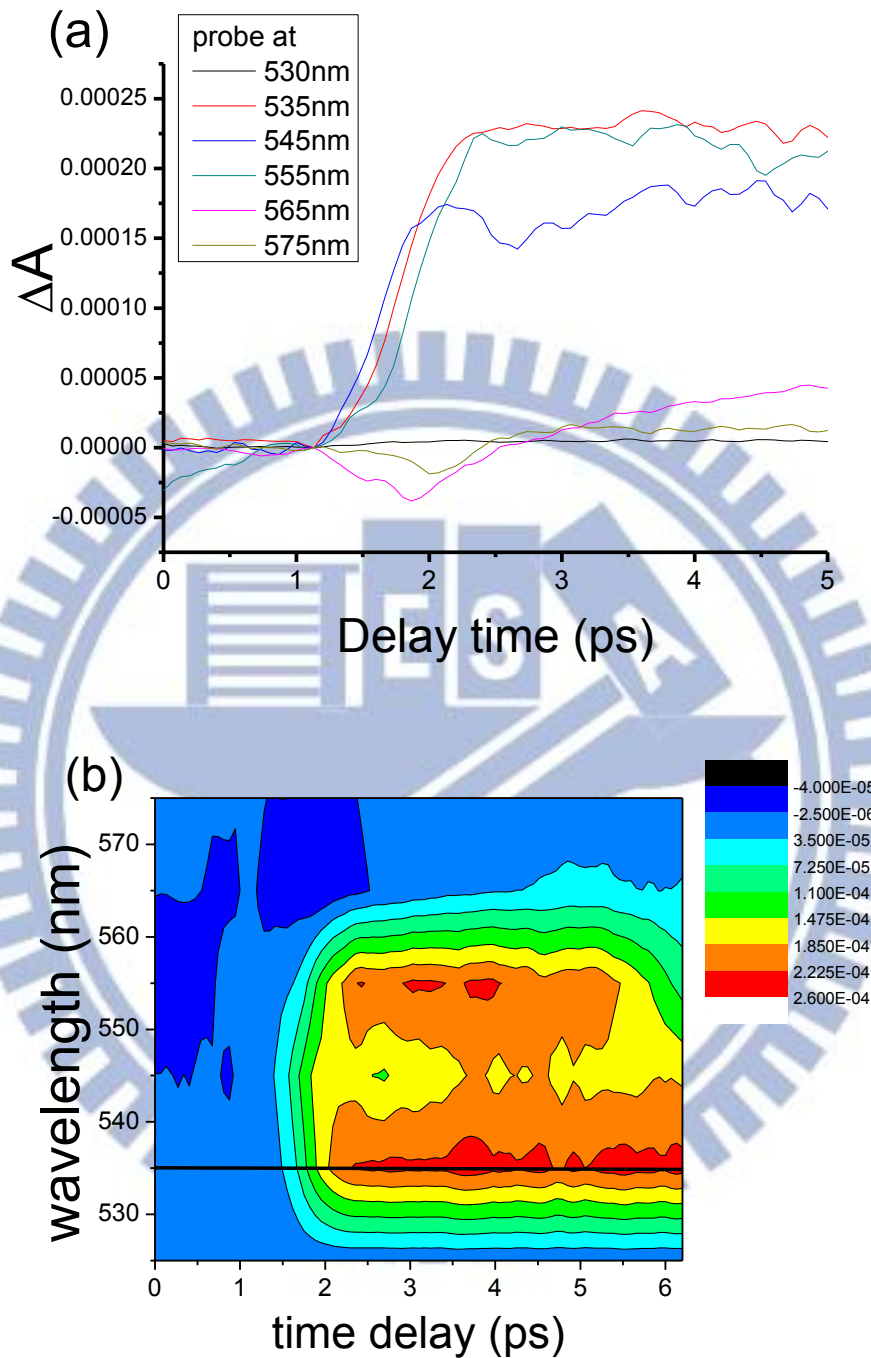
**Table 5-1. The peak position and band width of pure QDs and DTT treated film in 4 different sizes with peak variation.**

Size	CdSe solid		CdSe@DTT solid		peak shift (nm/meV)
	Peak (nm / eV)	width (nm)	Peak (nm / eV)	Width (nm)	
2.8nm	525.7/2.3585	47.4	534.3/2.3205	44.1	8.6/380
2.8nm	524.5/2.3639	54.2	535.3/2.3162	46.6	10.8/477
3.1nm	543.6/2.2808	47.7	556.0/2.2299	39.7	12.4/509
3.5nm	564.8/2.1952	38.4	572.8/2.1645	40.5	8/307



**Figure 5-3. The schematic diagram shows a dithiol molecule DTT connect to two QDs enhanced QDs coupling.**

Following we present a study of ultrafast electron and hole dynamics in coupled CdSe/ZnS QD solids, focusing on the first few picoseconds after excitation. We distinguish two separate rate relaxation processes that occur on this time scale: hot carrier relaxation from higher levels to the  $1S$  electron and hole levels (intraband carrier cooling) and carrier relaxation due to hopping between different QDs (referred to as spectral diffusion). Figure 5-4 presents selected absorption transients for a QD / DTT film at a pump wavelength of 400nm and several probe wavelengths in the  $1S_h-1S_e$  profile. The probe wavelength dependence of the absorption transients for QD dispersions has been studied [52, 53]. In this plot, state filling (absorption bleach) and Coulomb interactions between multiple excitons (absorption shift), determine the transient absorption features. The strongly wavelength dependence, so-called biexciton shift, occurs both for hot carriers, directly after excitation, and for thermalized carriers. This is due to a red shift of the optical transitions upon photoexcitation. There are still many unknown and interesting part of electronic coupling of QDs film needed to be studied. The related researches could be a promising theme for future work.



**Figure 5-4. (a) Transient absorption spectra at low pump intensity  $\langle N_{\text{abs}} = 0.5 \rangle$  and various probe wavelengths near the  $1S_h - 1S_e$  transition for a QD / DTT film. (b) Contour plot of the same data for the QD / DTT film. The black line in (b) denotes the ground state absorption maximum.**



## 5-2 Summary

In summary, we have demonstrated the function of short-chain thiol-containing molecules capping on CdSe/ZnS quantum dots (QDs) in determination of their optical and electrical properties by employing time-resolved photoluminescence, temperature-dependent PL, transient absorption, and steady-state fluorescence measurements. The steady-state fluorescence spectra provided the critical concentration of thiol/thiolate or coordination-type bonds /covalent-type bonds conversion. The ultrafast transient absorption confirmed the electron dynamics and surface passivation immediately after thiol molecules are added. From temperature-dependent PL, the activation energy band gap (exciton binding energy), and surface electronic state distribution could be investigated. Finally, the time-resolved PL examined the hole dynamics after thiolate was formed. We found that thiol interact with QD only by weaker coordination-type bonds through the sulfur lone-pair electrons and passivate the surface of QDs by preventing core electron from defect sites on the surface. Another stronger covalent-type bonds are formed when thiol turn to thiolate through long time incubation, and the new hole traps would be produced. The schematic diagram was shown in Figure 5-5.

Different thiol-containing molecules were investigated and showed different performance. 1-propanethiol (NPM) exhibits little effect on the properties of QDs even though it is a short-chain thiol-containing molecule. One of possible reason is that other tested thiol molecules,  $\beta$ -Mercaptoethanol(BME) and 3-Mercaptopropionic acid (MPA) have smaller thiol  $pK_a$ , which determines the ability to transform into thiolate. Thus, the formation of covalent bonds of 1-propanethiol (NPM) with higher  $pK_a$  and QDs may be difficult. The second important reason would be the lack of second-order oxygen of NPM. Evidently, NPM without other lone-pairs compared to BME and MPA, cannot bind to QDs with coordination-type bonds effectively. Finally, the surface passivation

of QD happens as long as the QDs are surrounded by negative charges. For electron-rich molecules such as thiol, dithiol or gel with lone-pair, surface passivation ability has been confirmed. The schematic diagram is shown in Figure 5-6.

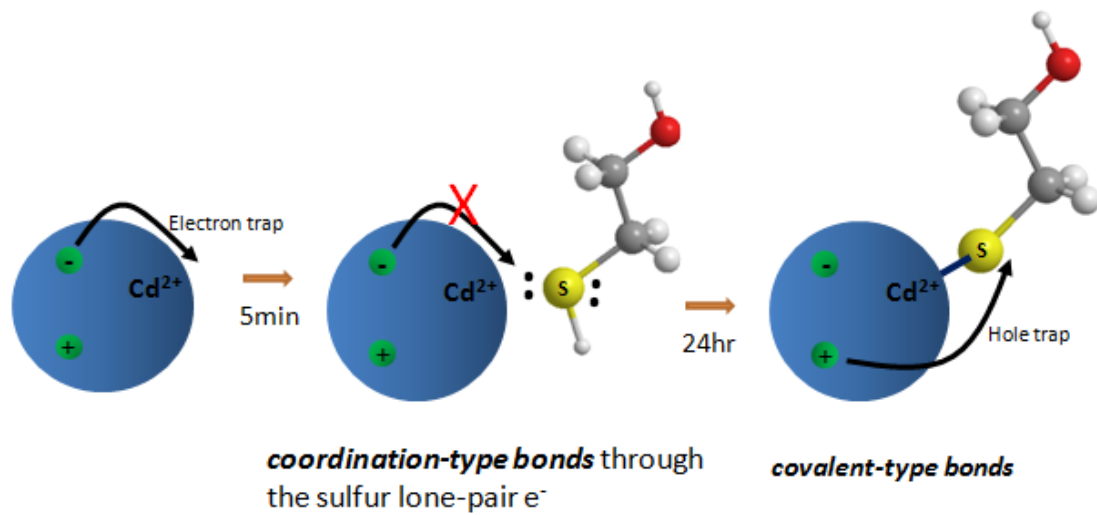
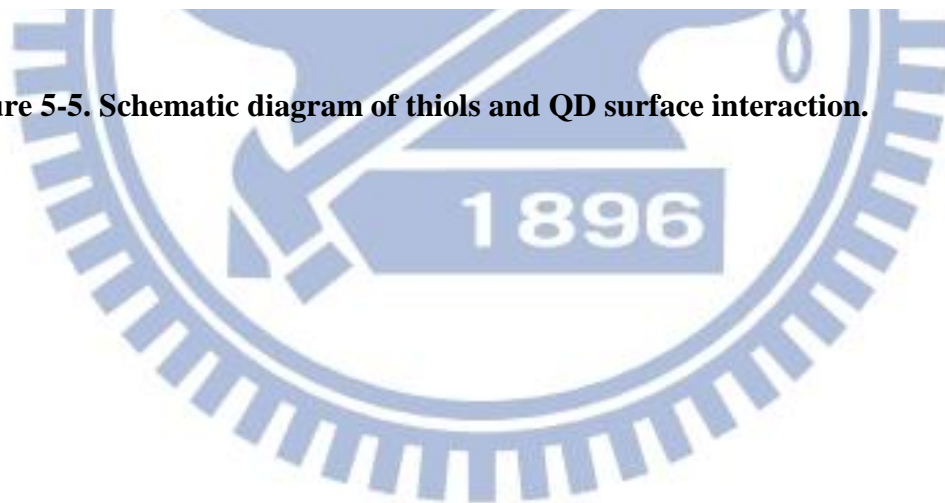
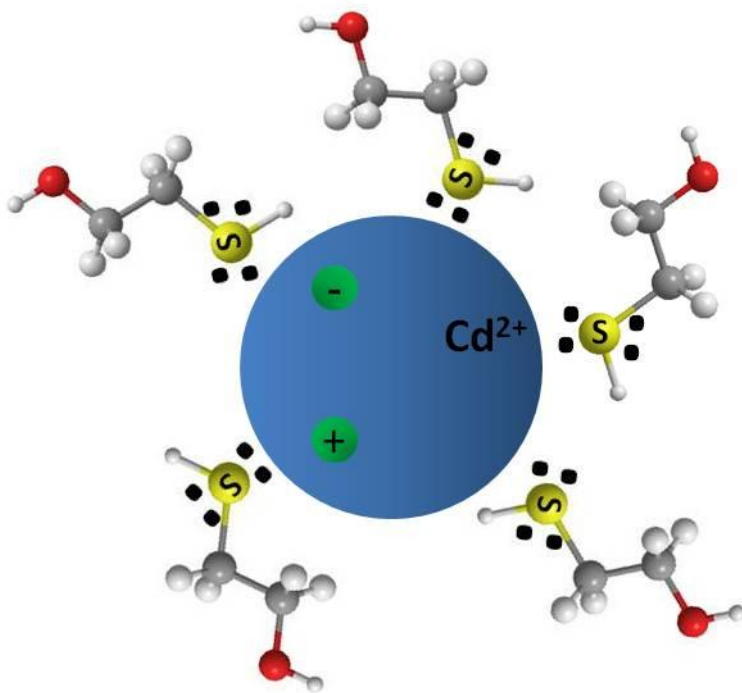
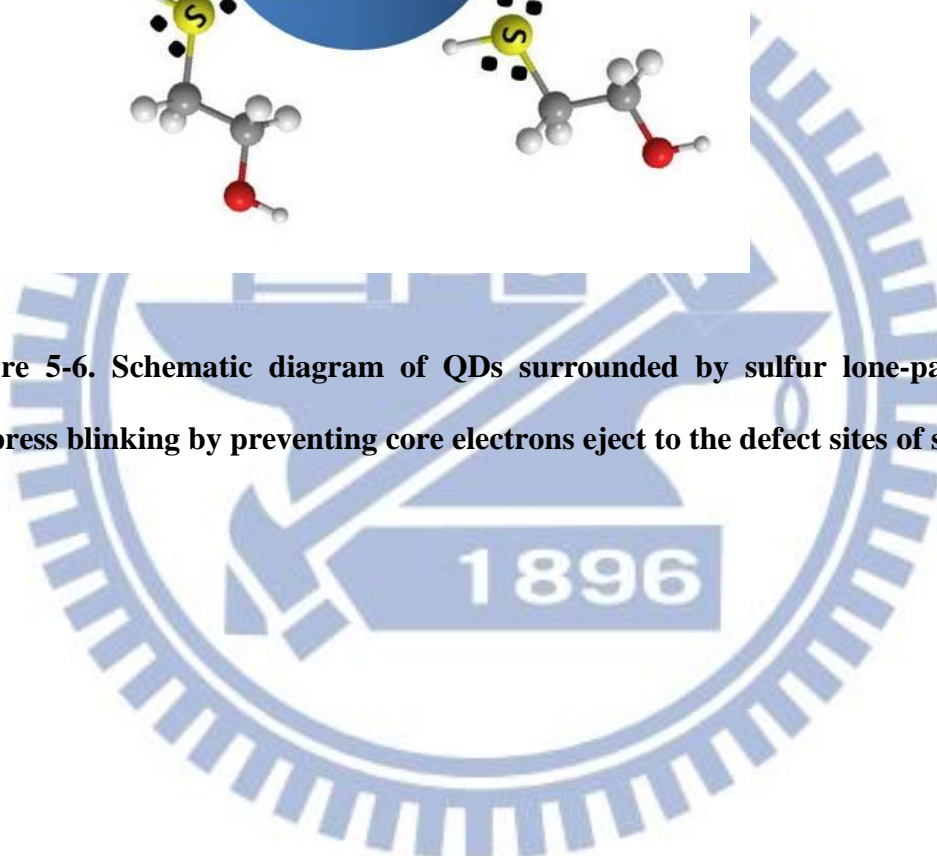


Figure 5-5. Schematic diagram of thiols and QD surface interaction.





**Figure 5-6. Schematic diagram of QDs surrounded by sulfur lone-pairs and suppress blinking by preventing core electrons eject to the defect sites of surface.**



## References

- [1] V. V. Matyilitsky, *et al.*, "Ultrafast Interfacial Charge Carrier Dynamics in ZnSe and ZnSe/ZnS Core/Shell Nanoparticles: Influence of Shell Formation," *The Journal of Physical Chemistry C*, vol. 112, pp. 2703-2710, 2008/02/01 2008.
- [2] R. P. Prasankumar, *et al.*, "Ultrafast carrier dynamics in semiconductor nanowires," *physica status solidi (b)*, vol. 246, pp. 1973-1995, 2009.
- [3] C. A. Nelson and X. Y. Zhu, "Reversible Surface Electronic Traps in PbS Quantum Dot Solids Induced by an Order–Disorder Phase Transition in Capping Molecules," *Journal of the American Chemical Society*, vol. 134, pp. 7592-7595, 2012/05/09 2012.
- [4] O. Chen, *et al.*, "Surface-Functionalization-Dependent Optical Properties of II–VI Semiconductor Nanocrystals," *Journal of the American Chemical Society*, vol. 133, pp. 17504-17512, 2011/11/02 2011.
- [5] M. Soreni-Harari, *et al.*, "Tuning Energetic Levels in Nanocrystal Quantum Dots through Surface Manipulations," *Nano Letters*, vol. 8, pp. 678-684, 2008/02/01 2008.
- [6] N. Yaacobi-Gross, *et al.*, "Molecular control of quantum-dot internal electric field and its application to CdSe-based solar cells," *Nat Mater*, vol. 10, pp. 974-979, 2011.
- [7] N. T. N. Truong, *et al.*, "Improvement of CdSe/P3HT bulk hetero-junction solar cell performance due to ligand exchange from TOPO to pyridine," *Solar Energy Materials and Solar Cells*, vol. 95, pp. 3009-3014, 2011.
- [8] A. Pandey and P. Guyot-Sionnest, "Slow Electron Cooling in Colloidal Quantum Dots," *Science*, vol. 322, pp. 929-932, November 7, 2008 2008.
- [9] W. A. Tisdale, *et al.*, "Hot-Electron Transfer from Semiconductor Nanocrystals," *Science*, vol. 328, pp. 1543-1547, June 18, 2010 2010.
- [10] M. A. Hines and P. Guyot-Sionnest, "Synthesis and Characterization of Strongly Luminescing ZnS-Capped CdSe Nanocrystals," *The Journal of Physical Chemistry*, vol. 100, pp. 468-471, 1996/01/01 1996.
- [11] S. Jeong, *et al.*, "Effect of the Thiol–Thiolate Equilibrium on the Photophysical Properties of Aqueous CdSe/ZnS Nanocrystal Quantum Dots," *Journal of the American Chemical Society*, vol. 127, pp. 10126-10127, 2005/07/01 2005.
- [12] S. Hohng and T. Ha, "Near-Complete Suppression of Quantum Dot Blinking in Ambient Conditions," *Journal of the American Chemical Society*, vol. 126, pp. 1324-1325, 2004/02/01 2004.

- [13] T. D. Krauss and J. J. Peterson, "Bright Future for Fluorescence Blinking in Semiconductor Nanocrystals," *The Journal of Physical Chemistry Letters*, vol. 1, pp. 1377-1382, 2010/05/06 2010.
- [14] O. Voznyy, "Mobile Surface Traps in CdSe Nanocrystals with Carboxylic Acid Ligands," *The Journal of Physical Chemistry C*, vol. 115, pp. 15927-15932, 2011/08/18 2011.
- [15] P. Kambhampati, "Unraveling the Structure and Dynamics of Excitons in Semiconductor Quantum Dots," *Accounts of Chemical Research*, vol. 44, pp. 1-13, 2011/01/18 2010.
- [16] V. I. Klimov, "Optical Nonlinearities and Ultrafast Carrier Dynamics in Semiconductor Nanocrystals," *The Journal of Physical Chemistry B*, vol. 104, pp. 6112-6123, 2000/07/01 2000.
- [17] H. S. Mansur, "Quantum dots and nanocomposites," *Wiley Interdisciplinary Reviews: Nanomedicine and Nanobiotechnology*, vol. 2, pp. 113-129, 2010.
- [18] D. Gerion, *et al.*, "Synthesis and Properties of Biocompatible Water-Soluble Silica-Coated CdSe/ZnS Semiconductor Quantum Dots<sup>†</sup>," *The Journal of Physical Chemistry B*, vol. 105, pp. 8861-8871, 2001/09/01 2001.
- [19] V. I. Klimov, "Spectral and Dynamical Properties of Multiexcitons in Semiconductor Nanocrystals," *Annual Review of Physical Chemistry*, vol. 58, pp. 635-673, 2007/05/01 2007.
- [20] A. M. Smith and S. Nie, "Semiconductor Nanocrystals: Structure, Properties, and Band Gap Engineering," *Accounts of Chemical Research*, vol. 43, pp. 190-200, 2010/02/16 2009.
- [21] D. F. Underwood, *et al.*, "Ultrafast Carrier Dynamics in CdSe Nanocrystals Determined by Femtosecond Fluorescence Upconversion Spectroscopy," *The Journal of Physical Chemistry B*, vol. 105, pp. 436-443, 2001/01/01 2000.
- [22] J. Antelman, *et al.*, "Suppression of Quantum Dot Blinking in DTT-Doped Polymer Films<sup>†</sup>," *The Journal of Physical Chemistry C*, vol. 113, pp. 11541-11545, 2009/07/09 2009.
- [23] M. Nirmal, *et al.*, "Fluorescence intermittency in single cadmium selenide nanocrystals," *Nature*, vol. 383, pp. 802-804, 1996.
- [24] K. T. Shimizu, *et al.*, "Blinking statistics in single semiconductor nanocrystal quantum dots," *Physical Review B*, vol. 63, p. 205316, 2001.
- [25] M. Kuno, *et al.*, "Nonexponential "blinking" kinetics of single CdSe quantum dots: A universal power law behavior," *The Journal of Chemical*

- Physics*, vol. 112, pp. 3117-3120, 2000.
- [26] P. Frantsuzov, *et al.*, "Universal emission intermittency in quantum dots, nanorods and nanowires," *Nat Phys*, vol. 4, pp. 519-522, 2008.
- [27] R. Verberk, *et al.*, "Simple model for the power-law blinking of single semiconductor nanocrystals," *Physical Review B*, vol. 66, p. 233202, 2002.
- [28] A. L. Efros and M. Rosen, "Random Telegraph Signal in the Photoluminescence Intensity of a Single Quantum Dot," *Physical Review Letters*, vol. 78, pp. 1110-1113, 1997.
- [29] R. G. Neuhauser, *et al.*, "Correlation between Fluorescence Intermittency and Spectral Diffusion in Single Semiconductor Quantum Dots," *Physical Review Letters*, vol. 85, pp. 3301-3304, 2000.
- [30] F. Koberling, *et al.*, "Fluorescence Anisotropy and Crystal Structure of Individual Semiconductor Nanocrystals<sup>†</sup>," *The Journal of Physical Chemistry B*, vol. 107, pp. 7463-7471, 2003/07/01 2003.
- [31] D. I. Chepic, *et al.*, "Auger ionization of semiconductor quantum drops in a glass matrix," *Journal of Luminescence*, vol. 47, pp. 113-127, 1990.
- [32] T. Kawashima, *et al.*, "Control of Surface Migration of Gold Particles on Si Nanowires," *Nano Letters*, vol. 8, pp. 362-368, 2008/01/01 2007.
- [33] S. A. Empedocles and M. G. Bawendi, "Influence of Spectral Diffusion on the Line Shapes of Single CdSe Nanocrystallite Quantum Dots," *The Journal of Physical Chemistry B*, vol. 103, pp. 1826-1830, 1999/03/01 1999.
- [34] B. Mahler, *et al.*, "Towards non-blinking colloidal quantum dots," *Nat Mater*, vol. 7, pp. 659-664, 2008.
- [35] X. Wang, *et al.*, "Non-blinking semiconductor nanocrystals," *Nature*, vol. 459, pp. 686-689, 2009.
- [36] M. G. Lupo, *et al.*, "Ultrafast Electron-Hole Dynamics in Core/Shell CdSe/CdS Dot/Rod Nanocrystals," *Nano Letters*, vol. 8, pp. 4582-4587, 2008/12/10 2008.
- [37] C. R. Carey, *et al.*, "Ultrafast Transient Absorption Measurements of Charge Carrier Dynamics in Single II-VI Nanowires," *The Journal of Physical Chemistry C*, vol. 113, pp. 19077-19081, 2009/11/05 2009.
- [38] X. Wen, *et al.*, "Temperature dependent spectral properties of type-I and quasi type-II CdSe/CdS dot-in-rod nanocrystals," *Physical Chemistry Chemical Physics*, vol. 14, pp. 3505-3512, 2012.
- [39] D. Valerini, *et al.*, "Temperature dependence of the photoluminescence properties of colloidal CdSe / ZnS core/shell quantum dots embedded in

- a polystyrene matrix," *Physical Review B*, vol. 71, p. 235409, 2005.
- [40] X. Wang, *et al.*, "Photoluminescence upconversion in colloidal CdTe quantum dots," *Physical Review B*, vol. 68, p. 125318, 2003.
- [41] G. Morello, *et al.*, "Temperature and Size Dependence of Nonradiative Relaxation and Exciton–Phonon Coupling in Colloidal CdTe Quantum Dots," *The Journal of Physical Chemistry C*, vol. 111, pp. 5846-5849, 2007/04/01 2007.
- [42] J. Z. Zhang, "Interfacial Charge Carrier Dynamics of Colloidal Semiconductor Nanoparticles," *The Journal of Physical Chemistry B*, vol. 104, pp. 7239-7253, 2000/08/01 2000.
- [43] P. Yu, *et al.*, "Temperature-Dependent Fluorescence in Au<sub>10</sub> Nanoclusters," *The Journal of Physical Chemistry C*, vol. 116, pp. 6567-6571, 2012/03/22 2012.
- [44] X. Wen, *et al.*, "Temperature dependent photoluminescence in oxygen ion implanted and rapid thermally annealed ZnO/ZnMgO multiple quantum wells," *Applied Physics Letters*, vol. 90, pp. 221914-3, 2007.
- [45] J. Shah, *Ultrafast spectroscopy of semiconductors and semiconductor nanostructures* vol. 115: Springer Verlag, 1999.
- [46] Y. P. Varshni, "Temperature dependence of the energy gap in semiconductors," *Physica*, vol. 34, pp. 149-154, 1967.
- [47] J. T. Darrow, *et al.*, "Power scaling of large-aperture photoconducting antennas," *Applied Physics Letters*, vol. 58, pp. 25-27, 1991.
- [48] S. Schmitt-Rink, *et al.*, "Theory of the linear and nonlinear optical properties of semiconductor microcrystallites," *Physical Review B*, vol. 35, pp. 8113-8125, 1987.
- [49] E. Rothenberg, *et al.*, "Electric Field Induced Switching of the Fluorescence of Single Semiconductor Quantum Rods," *Nano Letters*, vol. 5, pp. 1581-1586, 2005/08/01 2005.
- [50] J. M. Luther, *et al.*, "Multiple Exciton Generation in Films of Electronically Coupled PbSe Quantum Dots," *Nano Letters*, vol. 7, pp. 1779-1784, 2007/06/01 2007.
- [51] Y. Gao, *et al.*, "Enhanced Hot-Carrier Cooling and Ultrafast Spectral Diffusion in Strongly Coupled PbSe Quantum-Dot Solids," *Nano Letters*, vol. 11, pp. 5471-5476, 2011/12/14 2011.
- [52] M. T. Trinh, *et al.*, "Nature of the Second Optical Transition in PbSe Nanocrystals," *Nano Letters*, vol. 8, pp. 2112-2117, 2008/07/01 2008.
- [53] R. J. Ellingson, *et al.*, "Highly Efficient Multiple Exciton Generation in Colloidal PbSe and PbS Quantum Dots," *Nano Letters*, vol. 5, pp. 865-871,

2005/05/01 2005.

